THE ASTROPHYSICAL JOURNAL, 589:509–525, 2003 May 20
© 2003. The American Astronomical Society. All rights reserved. Printed in U.S.A.

# *CHANDRA* OBSERVATIONS OF ASSOCIATES OF $\eta$ CARINAE. I. LUMINOSITIES[1]

NANCY REMAGE EVANS, FREDERICK D. SEWARD, MIRIAM I. KRAUSS, TAKASHI ISOBE, JOY NICHOLS, ERIC M. SCHLEGEL, AND SCOTT J. WOLK
Smithsonian Astrophysical Observatory, MS 4, 60 Garden Street, Cambridge, MA 02138
*Received 2002 October 22; accepted 2003 January 22*

## ABSTRACT

The region around the $\eta$ Carinae Nebula has three OB associations, which contain a Wolf-Rayet star and several massive O3 stars. An early *Chandra* ACIS-I image was centered on $\eta$ Car and includes Trumpler 16 and part of Trumpler 14. The *Chandra* image confirms the well-known result that O and very early B stars are X-ray sources with $L_X \simeq 10^{-7} L_{bol}$ over an X-ray luminosity range of about 100. Two new, anomalously strong X-ray sources have been found among the hot star population: Tr 16-244, a heavily reddened O3 I star, and Tr 16-22, a heavily reddened O8.5 V star. Two stars have an unusually large $L_X/L_{bol}$: HD 93162, a Wolf-Rayet star (and possible binary), and Tr 16-22, a possible colliding-wind binary. In addition, a population of sources associated with cool stars is detected. In the color-magnitude diagram, these X-ray sources sit above the sequence of field stars in the Carina arm. The OB stars are on average more X-ray–luminous than the cool star X-ray sources. X-ray sources among A stars have X-ray luminosities similar to those of cooler stars and may be due to cooler companions. Upper limits are presented for B stars that are not detected in X-rays. These upper limits are also the upper limits for any cool companions that the hot stars may have. Hardness ratios are presented for the most luminous sources in bands 0.5–0.9, 0.9–1.5, and 1.5–2.04 keV. The available information on the binary nature of the hot stars is discussed, but binarity does not correlate with X-ray strength in a simple way.

*Subject headings:* open clusters and associations: individual (Trumpler 14, Trumpler 16) — X-rays: stars
*On-line material:* machine-readable tables

## 1. INTRODUCTION

The challenge of X-rays in O stars was posed by *Einstein X-Ray Observatory* observations of the Carina Nebula (Seward et al. 1979; Seward & Chlebowski 1982) and Cyg OB2 (Harnden et al. 1979). Four particularly strong sources were found in Trumpler 14 and Trumpler 16 (Tr 14 and Tr 16, respectively): $\eta$ Car itself, HD 93129A/B (O3 If), HD 93162 (=WR 25, a Wolf-Rayet [W-R] star), and HD 93250 (O3 V). All the bright O stars in the Einstein field were detected in X-rays. Among the clues to the source of X-rays was that $L_X$ is approximately 7 orders of magnitude smaller than $L_{bol}$ for all O stars. The W-R star WR 25 is unusually strong in X-rays compared with two other W-R stars in the region.

Several X-ray studies have been made subsequently, including Corcoran et al. (1995; *ROSAT* images) and Crowther, Hillier, & Smith (1995a), both of whom confirmed that WR 25 is unusually bright for a W-R star.

The region around $\eta$ Car is of considerable interest. $\eta$ Car itself is arguably the most massive star in the galaxy, with a history of luminosity variations. A *Hubble Space Telescope* image revealed a bipolar structure in the center of the nebula. The Carina Nebula contains the most massive stars in the Galaxy, with initial masses up to 120 $M_\odot$. Walborn (1971) invented the spectral classification O3 because several stars in this region are hotter than existing MK classifications. Recent studies include the Massey & Johnson study (1993, hereafter MJ93) of reddening from spectroscopy and photometry and the proper-motion study of Cudworth, Martin, & DeGioia-Eastwood (1993), which provides membership probability. The clusters Tr 14 and Tr 16 provide a snapshot of evolution of the most massive stars known. The evolutionary sequence in order of decreasing mass goes from $\eta$ Car through the O3 If star through O3 V stars. A particularly perplexing question in this scenario is how the W-R star WR 25 fits in. This is discussed at some length by MJ93. It should be more evolved than the O3 stars; however, it is less luminous. This statement, of course, depends on the bolometric corrections, which are difficult to determine for O stars and especially difficult for W-R stars.

WR 25 is classified as WN7+abs by MJ93. WN7+abs stars belong to the nitrogen sequence of W-R stars, which are the most luminous and least chemically evolved, as mass loss strips off outer layers of the original star. They still retain some hydrogen, and the "abs" designation indicates that there are absorption components in the upper Balmer lines. WN7+abs stars differ from Of stars only in having a stronger wind. As noted by Crowther et al. (1995b), WN7+abs stars are found only in the youngest clusters, in contrast to WN7 stars. The scenario put forward by Crowther et al. (1995a, 1995b), based on their spectroscopy, envisions that WN7+abs stars are part of the most massive sequence of stars, immediately following the evolutionary stage of Of stars but preceding WN7 stars. (WN8 stars belong to a less massive sequence containing stars that have already been luminous blue variables or red supergiants.) This scenario accords with the selection of objects in Tr 16 and Tr 14 (WN7+abs, O3 If*, O3 V, and cooler stars).

Tr 16 and Tr 14 contain some of the youngest and most massive stars known, and they have been well studied. For

[1] Based on observations made with the *Chandra X-Ray Observatory*.

the same reason, many of their parameters are extreme and also controversial. The distance, for instance, adopted by Davidson & Humphreys (1997) to $\eta$ Car itself is 2.3 kpc. MJ93 find 3.2 kpc from extensive spectroscopy and photometry. Among the problems in determining the distance to Tr 14 and Tr 16 are the form of the reddening law and whether the two clusters have the same age and distance. Walborn (1995) illustrates quantitatively how the reddening law affects the derived distance. For $R = A_V/E(B-V) = 3.5$, his distance to Tr 16 is 2.5 kpc. Crowther et al. (1995b) use 2.6 kpc in their discussion of the W-R star in Tr 14, WR 25. We adopt 2.5 kpc for this study.

Given the dramatic appearance of the nebulosity in optical images of the cluster, the reddening within Tr 14 and Tr 16 is surprisingly uniform. The values of $E(B-V)$ for the hot stars from MJ93 have a scatter of approximately $\pm 0.2$ mag, centered approximately on 0.55 mag. The form of the reddening law in the region, however, has been debated. This is discussed further in § 6. Bolometric corrections are similarly problematic in comparing very luminous hot stars with W-R stars.

A good overview of X-ray studies of O stars and W-R stars in the pre-*Chandra* era is provided by Willis & Crowther (1996). The search for correlations between X-ray luminosity and other parameters has been elusive, and it is summarized by Chlebowski (1989).

The observations of $\eta$ Car itself from the early *Chandra* image have already been discussed by Seward et al. (2001). We now turn to the stars in the surrounding region. The discussion is broken into two papers. The current paper discusses the source counts, luminosity distributions, and hardness ratios. The second paper will discuss the low-resolution spectra of the strongest sources. The current paper is broken up into sections on the observation, detected sources, cool stars, luminosity distributions, X-ray–to-bolometric luminosity ratios, diffuse emission, upper limits, and hardness ratios.

## 2. OBSERVATIONS

The early *Chandra* science image placed $\eta$ Car at the focus of the I3 chip of the ACIS-I detector. Instrumental details about the *Chandra* satellite are given in Weisskopf et al. (2002).

Unfortunately, the $\eta$ Car observation was obtained during the period when the energy resolution of the detector was degrading. It was also obtained at an instrumental temperature that has not been fully calibrated. This means that the ACIS instrumental low-resolution spectra have uncertainties in the energy scale. The intrinsic interest of the sources in this image, however, means that there is insight to be gained from an analysis of the image despite these limitations.

Figure 1 shows the image on the ACIS-I chips. $\eta$ Car itself is near the center of the image, with stars in Tr 16 particularly prominent to the south. Tr 14 is in the extreme upper right. The identification of several of the sources (hot stars) is provided in Figure 1.

The data were analyzed using the CXC CIAO (*Chandra* Interactive Analysis of Observations) software. The data were filtered on standard *ASCA* grades and checked for times of poor aspect (pointing stability); none were found. There were no significant background flares during the observation, giving a total good exposure time of 9.63 ks.

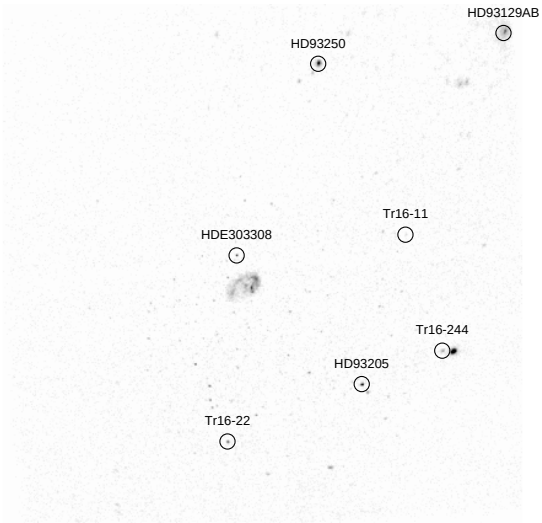



FIG. 1.—ACIS-I image with $\eta$ Car in the center. The image has been smoothed with a 1″ Gaussian. Tr 16 is in the center of the image; Tr 14 is in the upper right. A few of the sources are identified. The $16' \times 16'$ ACIS-I field is shown. North is up; east is to the left.

Sources were detected using the WAVDETECT program, which performs a Mexican hat wavelet decomposition and reconstruction.[2] WAVDETECT was run using scales of size 1, 2, 4, 8, and 16 pixels on an image that had been energy-filtered to contain data from 300 to 6000 eV. These choices maximized the number of total detections returned while minimizing the number of spurious detections.

The data were then split into three energy bands: 0.5–0.9, 0.9–1.5, and 1.5–2.04 keV. An exposure map was computed for the observation to take into account vignetting and chip gaps. A mean energy of 1.2 keV was used in generating the exposure map, which was normalized to its aim-point value. Source counts were extracted using the regions supplied by WAVDETECT. These counts were divided by the normalized mean exposure value and background-subtracted using data from an annulus centered on the source region. Sources within the background region were subtracted prior to this computation, and the area was adjusted accordingly.

The list of detected sources was culled in the following way to produce a list of significant sources. The distance off-axis for each source was calculated, and for this distance the size of the point-spread function (PSF) was determined. See, for instance, Figure 6.4 in the *Chandra* Proposers' Observatory Guide (2000).[3] (Specifically, a fit by J. Grimes 2001, private communication, for 80% encircled energy at 1.5 keV was used.) Background counts were measured in two areas of the image and found to be 0.045 counts arcsec$^{-2}$. The background within the PSF was calculated for each radius. For this background, the number of counts required for a 3 $\sigma$ detection was computed using the approximate formula from Gehrels (1986; "recommended approximation," p. 339). Using this approach, for instance, an on-axis source requires approximately 6 counts to be significant; a source 7′ off-axis requires approximately 12 counts.

[2] See the *CIAO* Detect Manual, chap. 13, at http://cxc.harvard.edu/ciao/download/doc/detect_html_manual.

[3] See http://cxc.harvard.edu/proposer/POG/html.

TABLE 1
X-RAY SOURCES: OB STARS

| Source | R.A. (J2000.0) | Decl. (J2000.0) | $R$ (arcmin) | All Energy Bands | | Soft Band | | Medium Band | | Hard Band | |
|---|---|---|---|---|---|---|---|---|---|---|---|
| | | | | Counts | Error | Counts | Error | Counts | Error | Counts | Error |
| 2..... | 10 45 16.55 | −59 43 36.9 | 3.0 | 84.7 | 9.1 | 43.5 | 6.6 | 33.9 | 5.7 | 7.3 | 2.6 |
| 5..... | 10 45 12.89 | −59 44 19.3 | 3.5 | 114.0 | 10.5 | 50.7 | 7.1 | 56.1 | 7.4 | 7.2 | 2.6 |
| 8..... | 10 45 08.23 | −59 40 49.2 | 0.6 | 32.6 | 5.7 | 12.6 | 3.6 | 20.0 | 4.5 | 0.0 | 0.0 |
| 9..... | 10 45 06.74 | −59 41 56.4 | 1.0 | 15.4 | 4.0 | 9.8 | 3.2 | 5.8 | 2.5 | −0.2 | 0.1 |
| 10..... | 10 45 05.90 | −59 40 05.8 | 1.0 | 232.1 | 15.3 | 141.4 | 11.9 | 73.7 | 8.6 | 17.0 | 4.1 |
| 22..... | 10 44 45.04 | −59 33 54.0 | 7.5 | 1572.8 | 37.2 | 597.6 | 23.0 | 771.7 | 26.0 | 203.5 | 13.4 |
| 25..... | 10 44 33.77 | −59 44 15.6 | 4.9 | 532.6 | 22.5 | 311.4 | 17.2 | 189.9 | 13.4 | 31.4 | 5.5 |
| 28..... | 10 44 10.38 | −59 43 11.3 | 7.0 | 4989.9 | 67.3 | 733.2 | 25.9 | 3018.1 | 52.3 | 1238.5 | 33.5 |
| 39..... | 10 45 20.61 | −59 42 51.0 | 2.8 | 19.9 | 4.4 | 8.2 | 2.8 | 10.8 | 3.2 | 0.9 | 1.0 |
| 44..... | 10 45 12.74 | −59 44 46.2 | 3.9 | 61.3 | 7.6 | 30.0 | 5.3 | 26.9 | 5.0 | 4.4 | 2.0 |
| 45..... | 10 45 12.26 | −59 45 00.6 | 4.1 | 64.4 | 7.9 | 30.0 | 5.4 | 28.1 | 5.2 | 6.3 | 2.5 |
| 55..... | 10 45 08.24 | −59 46 07.2 | 5.1 | 226.4 | 14.7 | 43.0 | 6.7 | 130.9 | 11.1 | 52.4 | 7.0 |
| 58..... | 10 45 05.86 | −59 43 07.6 | 2.1 | 27.0 | 5.2 | 14.9 | 3.9 | 12.1 | 3.5 | 0.0 | 0.0 |
| 59..... | 10 45 05.80 | −59 45 19.9 | 4.3 | 21.7 | 4.9 | 10.6 | 3.5 | 7.3 | 2.8 | 3.8 | 2.0 |
| 83..... | 10 44 47.37 | −59 43 53.3 | 3.5 | 52.2 | 7.2 | 37.1 | 6.1 | 11.1 | 3.3 | 4.1 | 2.0 |
| 88..... | 10 44 41.78 | −59 46 56.5 | 6.5 | 179.9 | 13.6 | 101.6 | 10.3 | 71.1 | 8.4 | 7.2 | 2.9 |
| 96..... | 10 44 32.31 | −59 44 31.2 | 5.3 | 108.9 | 10.1 | 80.4 | 8.7 | 27.6 | 5.1 | 0.8 | 1.0 |
| 102..... | 10 44 13.12 | −59 43 10.3 | 6.7 | 142.7 | 12.2 | 17.3 | 4.9 | 85.6 | 9.4 | 39.7 | 6.2 |
| 103..... | 10 43 57.73 | −59 32 53.2 | 11.7 | 2132.4 | 41.6 | 467.8 | 19.0 | 1240.4 | 31.7 | 424.2 | 19.0 |
| 135..... | 10 44 30.33 | −59 37 26.6 | 5.5 | 25.9 | 5.4 | 11.3 | 3.6 | 11.8 | 3.6 | 2.8 | 1.7 |
| 141..... | 10 44 22.62 | −59 39 25.3 | 5.4 | 13.3 | 4.8 | 1.2 | 2.7 | 8.5 | 3.3 | 3.5 | 2.0 |
| 145..... | 10 44 08.96 | −59 34 33.0 | 9.5 | 408.2 | 21.1 | 153.1 | 12.8 | 212.4 | 15.2 | 42.7 | 7.1 |
| 151..... | 10 44 38.27 | −59 32 55.8 | 8.7 | 112.6 | 15.1 | 68.1 | 11.1 | 37.0 | 9.0 | 7.5 | 4.8 |

NOTES.—Units of right ascension are hours, minutes, and seconds, and units of declination are degrees, arcminutes, and arcseconds. Table 1 is also available in machine-readable form in the electronic edition of the Astrophysical Journal.

The resulting sources are listed in Tables 1–4, separated by their optical identifications into OB stars (Table 4 of MJ93) and other sources. The other sources in the Table 2 lists are predominately pre–main-sequence stars. Sources within the $\eta$ Car Nebula have been omitted from the tables. As well as total counts from 0.5 to 2.04 keV, counts were measured in three energy bands, 0.5–0.9, 0.9–1.5, and 1.5–2.04 keV, referred to as soft ($S$), medium ($M$), and hard ($H$) bands, respectively. Errors are computed by DMEXTRACT using Poisson statistics. Tables 1 and 2 also list the radial distance $R$ from the aim point (in arcminutes).

Tables 3 and 4 list quantities derived from source counts, again divided into OB stars and other sources. Hardness ratios have been calculated from the three energy bands:

$$\mathrm{HR_{MS}} = \frac{M - S}{M + S} ,$$

$$\mathrm{HR_{HM}} = \frac{H - M}{H + M} .$$

Errors have been propagated from the errors on the energy bands.

In addition, fluxes and luminosities have been calculated from total count rates. PIMMS[4] was used to calculate a

[4] Portable Interactive Multi-Mission Simulator; see http://cxc.harvard.edu/toolkit/pimms.jsp.

TABLE 2
X-RAY SOURCES: NOT OB STARS

| Source | R.A. (J2000.0) | Decl. (J2000.0) | $R$ (arcmin) | All Energy Bands | | Soft Band | | Medium Band | | Hard Band | |
|---|---|---|---|---|---|---|---|---|---|---|---|
| | | | | Counts | Error | Counts | Error | Counts | Error | Counts | Error |
| 1..... | 10 45 22.01 | −59 40 52.5 | 2.3 | 23.7 | 4.9 | 3.9 | 2.0 | 15.8 | 4.0 | 4.0 | 2.0 |
| 3..... | 10 45 16.25 | −59 41 41.0 | 1.7 | 18.1 | 4.2 | 3.0 | 1.7 | 13.1 | 3.6 | 2.0 | 1.4 |
| 4..... | 10 45 14.80 | −59 40 07.1 | 1.7 | 12.9 | 3.6 | 3.9 | 2.0 | 6.9 | 2.6 | 2.0 | 1.4 |
| 6..... | 10 45 11.79 | −59 41 33.8 | 1.2 | 27.7 | 5.3 | 6.9 | 2.6 | 14.8 | 3.9 | 6.0 | 2.5 |
| 7..... | 10 45 08.57 | −59 40 16.7 | 1.0 | 27.9 | 4.9 | 8.1 | 2.6 | 16.3 | 3.7 | 3.5 | 1.7 |
| 11..... | 10 45 04.21 | −59 40 10.7 | 0.9 | 15.9 | 4.0 | 4.9 | 2.2 | 9.0 | 3.0 | 2.0 | 1.4 |
| 12..... | 10 45 03.89 | −59 38 19.9 | 2.7 | 20.9 | 4.5 | 4.2 | 2.0 | 13.6 | 3.6 | 3.1 | 1.7 |
| 14..... | 10 45 02.93 | −59 42 25.9 | 1.4 | 13.8 | 3.7 | 1.8 | 1.4 | 11.1 | 3.3 | 0.9 | 1.0 |
| 16..... | 10 44 52.79 | −59 43 19.1 | 2.6 | 37.1 | 6.1 | 7.7 | 2.8 | 21.3 | 4.6 | 8.1 | 2.8 |
| 17..... | 10 44 52.27 | −59 41 55.1 | 1.7 | 37.2 | 6.2 | 1.5 | 1.4 | 26.8 | 5.2 | 8.8 | 3.0 |

NOTES.—Units of right ascension are hours, minutes, and seconds, and units of declination are degrees, arcminutes, and arcseconds. Table 2 is published in its entirety in the electronic edition of the Astrophysical Journal. A portion is shown here for guidance regarding its form and content.

TABLE 3
X-RAY SOURCES: HARDNESS RATIOS: OB STARS

| Source | $HR_{MS}$ | | $HR_{HM}$ | | Flux | | Luminosity | |
|---|---|---|---|---|---|---|---|---|
| | Ratio | Error | Ratio | Error | log Flux (ergs cm$^{-2}$ s$^{-1}$) | Error (ergs cm$^{-2}$ s$^{-1}$) | log $L_X$ (ergs s$^{-1}$) | Error (ergs s$^{-1}$) |
| 2 | −0.12 | 0.14 | −0.65 | 0.20 | −12.91 | −13.88 | 31.96 | 30.99 |
| 5 | 0.05 | 0.12 | −0.77 | 0.17 | −12.78 | −13.82 | 32.09 | 31.06 |
| 8 | 0.23 | 0.22 | −1.00 | ... | −13.33 | −14.08 | 31.55 | 30.79 |
| 9 | −0.26 | 0.32 | −1.07 | 0.62 | −13.65 | −14.24 | 31.22 | 30.64 |
| 10 | −0.31 | 0.08 | −0.63 | 0.14 | −12.47 | −13.66 | 32.40 | 31.22 |
| 22 | 0.13 | 0.03 | −0.58 | 0.04 | −11.64 | −13.27 | 33.23 | 31.61 |
| 25 | −0.24 | 0.05 | −0.72 | 0.09 | −12.11 | −13.49 | 32.76 | 31.39 |
| 28 | 0.61 | 0.02 | −0.42 | 0.02 | −11.14 | −13.01 | 33.73 | 31.86 |
| 39 | 0.14 | 0.28 | −0.84 | 0.39 | −13.54 | −14.20 | 31.33 | 30.67 |
| 44 | −0.06 | 0.16 | −0.72 | 0.23 | −13.05 | −13.96 | 31.82 | 30.91 |
| 45 | −0.03 | 0.16 | −0.64 | 0.22 | −13.03 | −13.94 | 31.84 | 30.93 |
| 55 | 0.51 | 0.10 | −0.43 | 0.09 | −12.49 | −13.67 | 32.39 | 31.20 |
| 58 | −0.11 | 0.24 | −1.00 | ... | −13.41 | −14.12 | 31.47 | 30.75 |
| 59 | −0.18 | 0.30 | −0.31 | 0.38 | −13.50 | −14.15 | 31.37 | 30.73 |
| 83 | −0.54 | 0.18 | −0.46 | 0.32 | −13.12 | −13.98 | 31.75 | 30.89 |
| 88 | −0.18 | 0.09 | −0.82 | 0.15 | −12.59 | −13.71 | 32.29 | 31.17 |
| 96 | −0.49 | 0.12 | −0.94 | 0.26 | −12.80 | −13.84 | 32.07 | 31.04 |
| 102 | 0.66 | 0.13 | −0.37 | 0.11 | −12.69 | −13.75 | 32.19 | 31.12 |
| 103 | 0.45 | 0.03 | −0.49 | 0.03 | −11.51 | −13.22 | 33.36 | 31.65 |
| 135 | 0.02 | 0.27 | −0.61 | 0.35 | −13.43 | −14.11 | 31.45 | 30.77 |
| 141 | 0.75 | 0.53 | −0.41 | 0.39 | −13.72 | −14.16 | 31.16 | 30.71 |
| 145 | 0.16 | 0.07 | −0.66 | 0.08 | −12.23 | −13.52 | 32.65 | 31.36 |
| 151 | −0.30 | 0.15 | −0.66 | 0.26 | −12.79 | −13.66 | 32.09 | 31.21 |

NOTE.—Table 3 is also available in machine-readable form in the electronic edition of the Astrophysical Journal.

conversion from counts to energy. The count rates were calculated on the basis of 9.630 ks of good time. A Raymond-Smith plasma model spectrum with $\log T = 6.65$ was used, a spectrum typical of a stellar source found in young associations. The extinction is fairly uniform over the field. A column of $N_H = 3 \times 10^{21}$ cm$^{-2}$ was adopted, corresponding to $E(B-V) = 0.52$ mag, which is typical of the field (MJ93). With these parameters, a conversion factor of $1.4 \times 10^{-11}$ ergs cm$^{-2}$ s$^{-1}$ (counts s$^{-1}$) was derived. Conversion factors differed by less than a factor of 2 for a range of $\log T$ from 6.4 to 7.1. Luminosities were derived from fluxes using a distance of 2.5 kpc.

### 2.1. *Hot Stars*

Figure 2 shows the ACIS-I image of $\eta$ Car overlaid with the detected sources. Extensive optical work has been done on the clusters in the vicinity of $\eta$ Car, most recently by MJ93 and Cudworth et al. (1993). Table 4 in MJ93, a list of the brightest and bluest stars near $\eta$ Car, has been used to identify O and B stars with X-ray sources (*circles*). Sources that are not identified with O or B stars are shown as diamonds. (Note that the increase in the PSF of sources that are farther off-axis is not reflected in the plotting symbols.) Presumably, most of the X-ray sources that are not O stars

TABLE 4
X-RAY SOURCES: HARDNESS RATIOS: NOT OB STARS

| Source | $HR_{MS}$ | | $HR_{HM}$ | | Flux | | Luminosity | |
|---|---|---|---|---|---|---|---|---|
| | Ratio | Error | Ratio | Error | log Flux (ergs cm$^{-2}$ s$^{-1}$) | Error (ergs cm$^{-2}$ s$^{-1}$) | log $L_X$ (ergs s$^{-1}$) | Error (ergs s$^{-1}$) |
| 1 | 0.60 | 0.29 | −0.60 | 0.29 | −13.47 | −14.15 | 31.41 | 30.73 |
| 3 | 0.62 | 0.32 | −0.73 | 0.34 | −13.58 | −14.21 | 31.29 | 30.66 |
| 4 | 0.28 | 0.38 | −0.55 | 0.43 | −13.73 | −14.28 | 31.14 | 30.59 |
| 6 | 0.36 | 0.27 | −0.43 | 0.28 | −13.40 | −14.12 | 31.48 | 30.76 |
| 7 | 0.34 | 0.24 | −0.64 | 0.28 | −13.39 | −14.15 | 31.48 | 30.72 |
| 11 | 0.29 | 0.33 | −0.64 | 0.39 | −13.64 | −14.24 | 31.24 | 30.64 |
| 12 | 0.53 | 0.30 | −0.63 | 0.31 | −13.52 | −14.19 | 31.36 | 30.69 |
| 14 | 0.73 | 0.37 | −0.84 | 0.39 | −13.70 | −14.27 | 31.17 | 30.61 |
| 16 | 0.47 | 0.24 | −0.45 | 0.23 | −13.27 | −14.06 | 31.60 | 30.82 |
| 17 | 0.89 | 0.26 | −0.50 | 0.21 | −13.27 | −14.05 | 31.61 | 30.82 |

NOTE.—Table 4 is published in its entirety in the electronic edition of the Astrophysical Journal. A portion is shown here for guidance regarding its form and content.

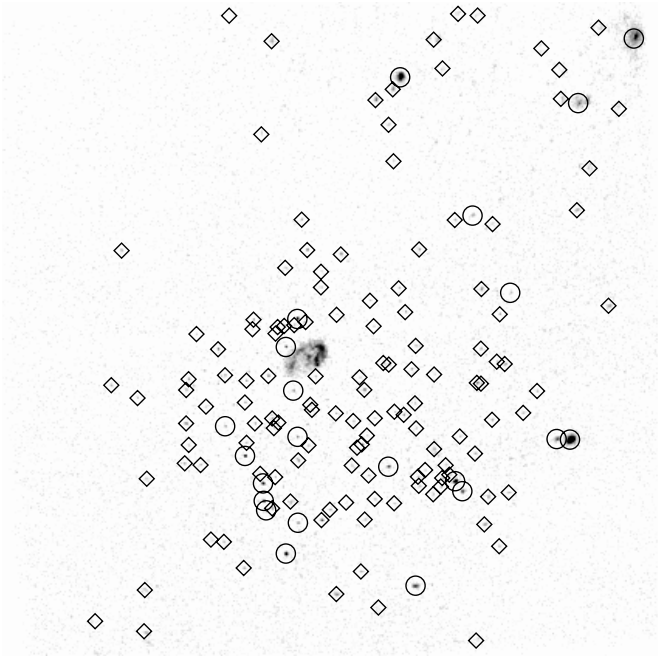


FIG. 2.—Sources found in the $\eta$ Car image. Sources identified with O or B stars are marked with circles, other sources with diamonds. All the symbols are the same size, although the source PSF is larger off-axis.

are pre–main-sequence stars, although very rarely they could be background objects, or even extragalactic sources.

Figure 3 shows the ACIS-I image of $\eta$ Car with the O and early B stars from the MJ93 list marked. It is clear that many of the X-ray sources are early-type stars, but many are not. Furthermore, many of the stars on the O and early B star list are not X-ray sources.

Figure 4 shows a plot of $V$ magnitude versus spectral type of the O and early B stars from the list of MJ93. (A few of the hot stars are not plotted because spectral types are not available.) The observed $V$ magnitude has not been

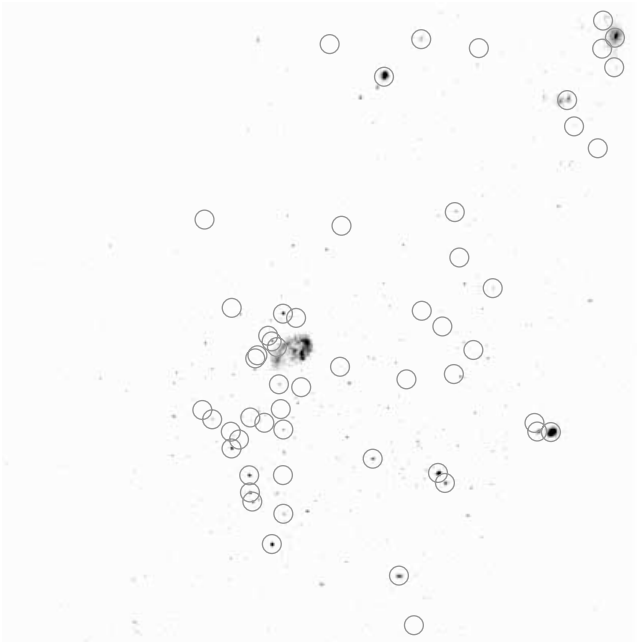


FIG. 3.—The $\eta$ Car image with the positions of known O and early B stars overlaid (*circles*).

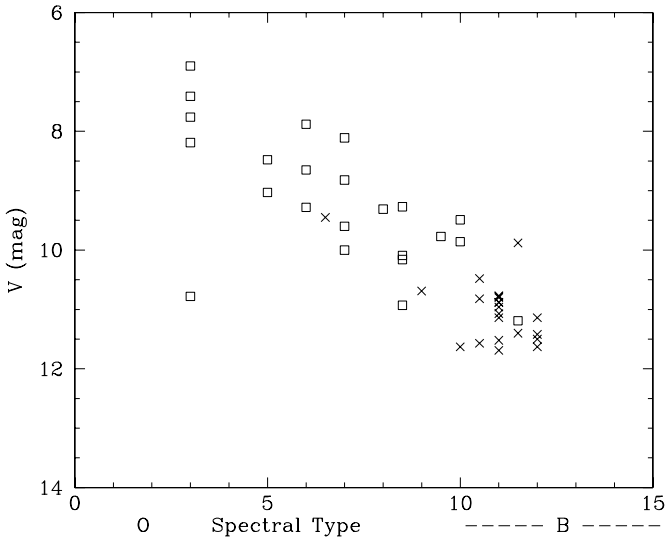



FIG. 4.—O and B stars on the $\eta$ Car ACIS-I image. Spectral type and $V$ magnitude are taken from MJ93. Squares mark detected X-ray sources, and crosses mark sources not detected in X-rays. Spectral type classes are sequential from 0 to 9 for O stars and from 10 to 15 for B stars.

corrected for reddening. However, extinction is fairly uniform over the field, so the pattern is not changed much if $V_0$ is used instead. An exception to this statement is the O3 star at 10.78 mag. This star was recognized by MJ93 to be unusually heavily reddened (Tr 16-244) and is discussed further below. The O6.5 star that is shown as not detected lies in the extreme upper right-hand corner of the ACIS-I image (Fig. 1 or 2), considerably off-axis, where a modest source could easily fail our detection criterion. With this exception, the dividing line between detections and nondetections is very sharp at approximately B0. This confirms previous results for O stars.

There is one B1.5 star that is detected in X-rays. A sole exception like this could easily result from a later companion. It will be discussed in § 6.

Figure 5 shows the total X-ray counts (Table 1) as a function of spectral type for the hot stars.

### 2.2. *Cool Stars*

The field corresponding to the *Chandra* image of $\eta$ Car was observed 2001 January 9–10 using the 0.9 m telescope at CTIO. The Tek-2K CCD has a 13′.5 field of view. First, four pointings, arrayed in a cruciform pattern with $\eta$ Car near the edge of each field, were used to observe the entire field. Johnson $B$ and $V$ filters and a Kron-Cousins $I$ filter were used, with exposures of 2 minutes each. This gives a limiting magnitude of about 19 at $V$. We performed an additional exposure of 10 minutes with each filter, centered on $\eta$ Car. This gave us a limiting magnitude of about 20.5 at $V$ within 6′.75 of the aim point.

Basic data reduction was handled using the QUADPROC package within IRAF[5] to bias-correct and flat-field the data. Fluxes for all standards and target stars were

[5] IRAF is distributed by the National Optical Astronomy Observatory, which is operated by the Association of Universities for Research in Astronomy (AURA), Inc., under contract to the National Science Foundation.

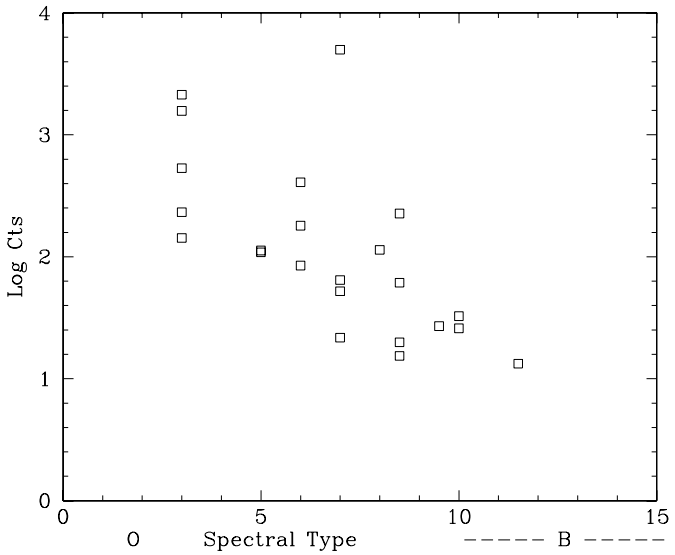



FIG. 5.—Hot stars detected on the $\eta$ Car ACIS-I image. Counts are the total counts. The W-R star (log counts = 3.7) has been arbitrarily plotted at O7 for comparison.

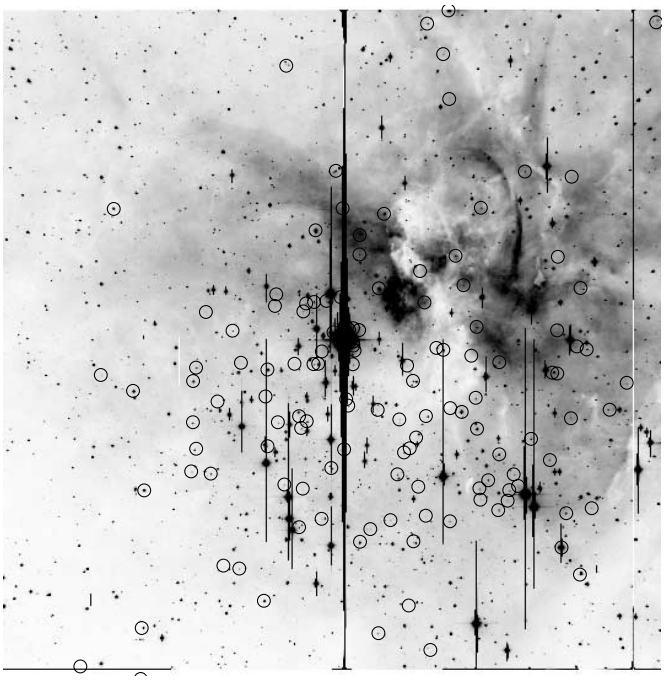


FIG. 6.—$V$ image of the center of the ACIS-I image. This image is approximately $12' \times 12'$ centered on $\eta$ Car. Circles mark the positions of X-ray sources, omitting X-ray sources that have been identified with OB stars. Most, but not all, of the circles contain a star, indicating that a cool star is the source of the X-rays. The image was taken with the 0.9 m telescope at CTIO by N. Huelamo and produced by one of the authors (T. I.).

determined using the "fitpsf" tool within the IRAF APPHOT package. Using this tool, fluxes were derived from the analytic fit to each individual PSF in lieu of simple aperture photometry. Stellar magnitudes and colors were put on the standard system using the PHOTCAL package. There were three difficulties encountered during data analysis. First, the region has a highly variable diffuse background. Second, $\eta$ Car and other bright stars make photometric measurements of stars in their proximity difficult. Finally, the region is quite crowded, and often faint stars have overlapping PSFs. Optical data are presented in Table 5, ordered by source number from Tables 2 and 4. Problems are noted as appropriate according to the codes at the end of the table. Photometric errors were determined using fits to the standard stars and by comparing observed values of target stars observed multiple times in separate pointings. This gives a more realistic assessment of the errors, given the highly variable and confused nature of the field. Errors are less than 5% at $V$ and less than 8.3% in the colors down to the completeness limits. These errors are somewhat conservative, because a star near the center of one field is on the edge of the comparison field; thus, the PSFs may differ greatly.

The central image with the X-ray sources overlaid is shown in Figure 6. The resulting color-magnitude diagram is shown in Figure 7. In this figure, X-ray sources near Tr 16 are shown as asterisks, and those near Tr 14 are shown as

TABLE 5
PHOTOMETRY OF LOW-MASS X-RAY SOURCES

| X-Ray ID | R.A. (J2000.0) | Decl. (J2000.0) | $B-V$ (mag) | $V$ (mag) | $V-I$ (mag) | Notes[a] |
|---|---|---|---|---|---|---|
| 1..... | 10 45 22.01 | −59 40 52.5 | 1.589 | 16.914 | 1.930 | |
| 3..... | 10 45 16.25 | −59 41 41.0 | 0.421 | 13.377 | 0.770 | |
| 4..... | 10 45 14.80 | −59 40 07.1 | ... | 18.452 | 1.734 | |
| 6..... | 10 45 11.79 | −59 41 33.8 | 2.009 | 19.178 | 2.054 | |
| 7..... | 10 45 08.57 | −59 40 16.7 | 1.106 | 15.410 | 1.350 | |
| 11..... | 10 45 04.21 | −59 40 10.7 | ... | ... | ... | 3 |
| 12..... | 10 45 03.89 | −59 38 19.9 | ... | ... | ... | 3 |
| 14..... | 10 45 02.93 | −59 42 25.9 | 1.759 | 17.852 | 2.058 | 3 |
| 16..... | 10 44 52.79 | −59 43 19.1 | 1.514 | 17.553 | 1.828 | 1b |
| 17..... | 10 44 52.27 | −59 41 55.1 | 1.089 | 15.610 | 1.474 | |

NOTE.—Units of right ascension are hours, minutes, and seconds, and units of declination are degrees, arcminutes, and arcseconds. Table 5 is published in its entirety in the electronic edition of the Astrophysical Journal. A portion is shown here for guidance regarding its form and content.

[a] Problem codes: (1) Two stars. (1a) Not resolved; not plotted. (1b) Not resolved; estimated combined magnitude. (1c) Resolved; position match poor; not plotted. (1d) Resolved; likely source used. (2) High background. (3) Contamination from nearby bright star. (4) Uncertain identification. (5) Faint star. (6) The star is overexposed. $V < 12.5$. (7) Outside the observed fields.

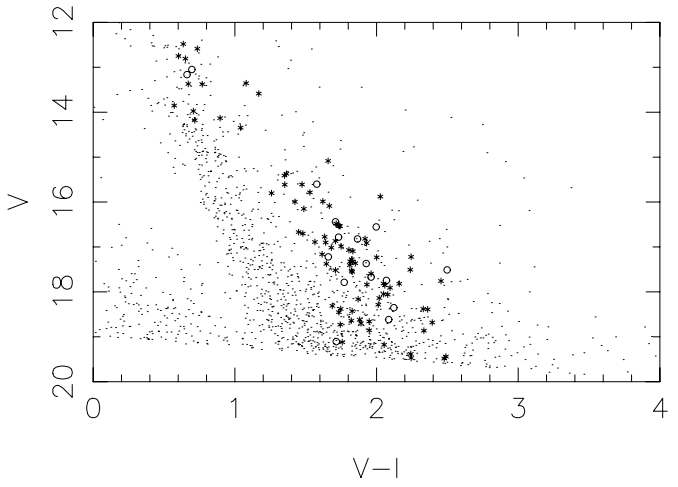



FIG. 7.—$V$ vs. $V-I$ color-magnitude diagram from the field in Fig. 6. X-ray sources associated with Tr 16 are marked with asterisks, X-ray sources associated with Tr 14 with circles, and other stars with dots. The dots define a main sequence, presumably of field stars in the Carina arm. The X-ray sources form a sequence that is more luminous than the field star sequence for cooler stars but coincides with it for hotter stars. This is what would be expected if the X-ray sources are pre–main-sequence stars. $V$ and $(V-I)$ are in magnitudes in all figures.

open circles. Other sources are shown as small dots. There are 6219 stars plotted. All stars detected in $B$, $V$, and $I$ and brighter than our completeness limit in the deep center field exposure are plotted. Figure 7 shows no significant difference between the age inferred for the Tr 16 sources compared with those near Tr 14, although the statistics are small. The figure demonstrates that the color-magnitude diagram easily distinguishes stars of the Carina arm of the Galaxy from nearby stars. The X-ray sources are all in a band about 1 mag wide, located about 1 mag above the field stars in the Carina arm. The well-defined sequence of field stars (*dots*) results because they, like the cluster stars, are concentrated in the Carina arm. Heavy obscuration behind the clusters restricts background contamination. The large spread among the stars is similar to that seen in Orion and is common among stars less than 1 Myr old, when small differences in age can lead to large differences in luminosity. About 100 stars in this region of the H-R diagram are not detected in X-rays. There are a few X-ray sources about 0.75 mag above the upper envelope of the X-ray population; we interpret these as binary stars. The reddest stars have $V-I$ of about 2. Given $A_V = 1.95$, the dereddened $V-I$ at $V = 19$ is 1.28. At an age of 1 Myr, this corresponds to a mass of about 1.15 $M_\odot$ (Baraffe et al. 1998).

## 3. LUMINOSITY DISTRIBUTION

Figure 8 shows the X-ray luminosity distribution of the O and early B stars (Table 3). Figure 9 shows the luminosity distribution for all sources that are not identified as OB stars (Table 4), the pre–main-sequence stars. A or B stars with later companions might be included, as could any extragalactic objects, but Figure 9 is heavily dominated by late-type stars. The luminosity distribution is distinctly different between these two groups. Most of the OB stars have luminosities greater than $10^{31}$ ergs s$^{-1}$. The cooler stars have luminosities strongly peaked at $10^{31}$ ergs s$^{-1}$, with the luminosity distribution of cool stars (Fig. 9) truncated at the faint end because of the relatively shallow X-ray image. As discussed in § 8, the depth of the X-ray exposure allowed all O stars near the image center to be detected.

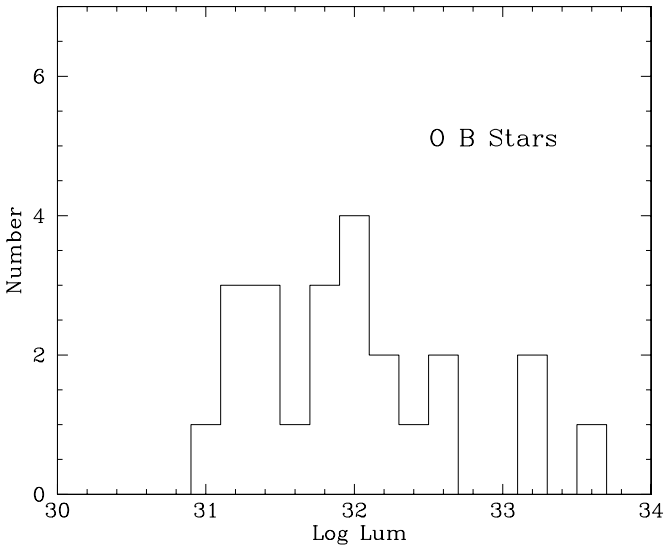



FIG. 8.—Luminosity distribution of OB stars. Luminosity is in units of ergs s$^{-1}$.

## 4. X-RAY LUMINOSITY FRACTION

### 4.1. *Hot Stars*

In this section we explore the efficiency of X-ray production from hot stars (Table 6). The first column is the optical identification, taken from Table 4 of MJ93. The second column is the X-ray source number from Table 3. Columns (3) and (5) are the $V$ and $E(B-V)$ (in magnitudes), again from MJ93. Column (4) is the spectral type. The reader is referred to Table 4 of MJ93 for the comparison of spectral types from different sources, and in some cases more complex spectral types. Recently, Walborn et al. (2002) have comprehensively reexamined

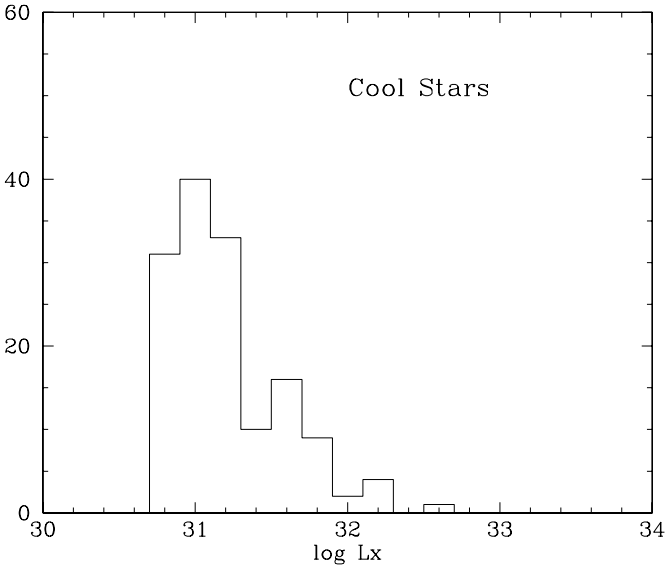



FIG. 9.—Luminosity distribution of sources not identified as O and early B stars. Luminosity is in units of ergs s$^{-1}$.

TABLE 6
X-Ray Sources: Hot Star Identifications

| Source (1) | Table 3 ID (2) | $V$ (mag) (3) | Spectral Type (4) | $E(B-V)$ (mag) (5) | $M_{bol}$ (mag) (6) | $\log(L_X/L_{bol})$ (7) |
|---|---|---|---|---|---|---|
| HD 93129A/B | 103 | 6.90 | O3 I | 0.55 | −11.5 | −6.72 |
| HD 93250 | 22 | 7.41 | O3 V | 0.49 | −10.7 | −6.54 |
| HD 93205 | 25 | 7.76 | O3 V | 0.40 | −10.1 | −6.76 |
| HD 93160 | 145 | 7.88 | O6 III | 0.31 | −9.4 | −6.60 |
| HD 93162 | 28 | 8.11 | WN7+abs | 0.66 | −10.1 | −5.40 |
| HDE 303308 | 10 | 8.19 | O3 V | 0.46 | −9.8 | −7.00 |
| HD 93204 | 96 | 8.48 | O5 V | 0.41 | −9.0 | −7.02 |
| CPD −59°2600 | 88 | 8.65 | O6 V | 0.51 | −9.0 | −6.80 |
| CPD −59°2603 | 83 | 8.82 | O7 V | 0.46 | −8.5 | −7.14 |
| HDE 303311 | 151 | 9.03 | O5 V | 0.45 | −8.6 | −6.84 |
| CPD −59°2635 | 44 | 9.27 | O8.5 V | 0.54 | −8.0 | −6.86 |
| CPD −59°2641 | 2 | 9.28 | O6 V | 0.61 | −8.7 | −7.00 |
| CPD −59°2636 | 5 | 9.31 | O8 V | 0.60 | −8.3 | −6.72 |
| CPD −59°2628 | 8 | 9.49 | B0 V | 0.44 | −7.5 | −6.94 |
| HD 93343 | 45 | 9.60 | O7 V | 0.56 | −8.0 | −6.84 |
| Tr 16-9 | 58 | 9.77 | O9.5 V | 0.56 | −7.2 | −6.89 |
| Tr 16-10 | 135 | 9.86 | B0 V | 0.57 | −6.9 | −6.80 |
| Tr 16-23 | 59 | 10.00 | O7 V | 0.69 | −7.5 | −7.12 |
| Tr 16-115 | 39 | 10.09 | O8.5 V | 0.46 | −6.8 | −6.88 |
| Tr 16-3 | 9 | 10.16 | O8.5 V | 0.52 | −6.9 | −7.02 |
| Tr 16-244 | 102 | 10.78 | O3 I | 0.94 | −8.6 | −6.34 |
| Tr 16-22 | 55 | 10.93 | O8.5 V | 0.78 | −6.8 | −5.82 |
| Tr 16-11 | 141 | 11.19 | B1.5 V | 0.43 | −4.9 | −6.28 |

the spectral classification of luminous stars. They make small adjustments to some classifications, including introducing new classes O2 and O3.5. The new classifications for stars in Table 5 are HD 93129A: O2 If*, HD 93129B: O3.5 V((f+)) HD 93250: O3.5 V((f+)), HD 93205: O3.5 V((f+)), and HDE 303308: O4 V((f+)). This finer gradation would only mildly affect the figures below. The sixth column is the bolometric magnitude, taken from Table 3 of Massey, DeGioia-Eastwood, & Waterhouse (2001) where available, made fainter by 0.56 mag because of the different distance assumed. (The X-ray–to-bolometric luminosity ratio that we use below, of course, does not depend on the distance.) For other stars, bolometric corrections were computed from the same formulae (Massey, Waterhouse, & DeGioia-Eastwood 2000). The final column is the log of the ratio of X-ray luminosity to the bolometric luminosity. Some of the sources in Table 6 have been identified in Figure 1.

While the reddening through the cluster field is reasonably uniform (MJ93), there have been studies that have suggested that the reddening law is unusual (see, e.g., Herbst 1976). Other studies have refuted this or concluded that only some objects have unusual reddening laws (Turner & Moffat 1980; Tapia et al. 1988).

One case in which the reddening law does appear to be unusual is the W-R star HD 93162 (=WR 25), although the unusual spectrum of the W-R star presents a problem in reddening determination. Crowther et al. (1995b) discuss the flux distribution from *IUE* through the IR and conclude that the reddening law for WR 25 is unusual [$E(B-V) = 0.66$ with $R = 4.6$]. This is the reddening that we adopt. The unusual spectrum also complicates the determination of the bolometric correction. We adopt the bolometric magnitude from Crowther et al. (1995a), −10.1 mag. (A small correction has been included for the difference between the distance they use and the one used here.)

There are a few unusual stars among the hot X-ray sources. Tr 16-244 is a faint star with an early spectral type (O3–O4 If). MJ93 took particular care in their observations because of this and because the star lies close to the bright W-R star HD 93162. Tr 16-244 is marked in Figure 1, and the W-R star is just to the right. The reddening implied for Tr 16-244 by the spectral type and photometry of MJ93 is larger than that of other stars in the cluster, with $E(B-V) = 0.94$ mag (using the relations in Massey et al. 2000). Tr 16-244 and HD 93162 both lie very close to the band of obscuration in the visual image. However, the W-R star is between Tr 16-244 and the dust lane. While reddening is difficult to determine for W-R stars, the value found by Crowther et al. (1995b) for the total extinction in the visual of the W-R star, ($A_V = 3.0$ mag) is very close to that for Tr 16-244. Thus, it is not clear whether the large reddening for those two stars is caused by the dust lane or could have a circumstellar component (for each star). For Tr 16-244, since the spectral type is the same as for HD 93129A/B, the same temperature and bolometric correction were used in creating Table 6. The resulting $M_{bol}$ is −8.6 mag, although there are obviously several sources of uncertainty in this number.

The other hot star with surprising photometry is Tr 16-22. The $V$ magnitude is faint for a spectral type of O8.5 V, suggesting a high reddening. Tr 16-22 is very close to the dust lane that cuts diagonally through the lower left of the image (Fig. 1), so the foreground absorption may be particularly large for this star. The spectrum MJ93 shows is similar to other O8.5 V spectra, except that the lines are slightly shallower and broader. However, the value of $Q$ from the photometry gives rather unconvincing values for temperature and bolometric correction. Comparing the $B-V$ and

$U-B$ values from MJ93 with those of Herbst (1976) and Feinstein (1969) shows that the agreement between the latter two is much better. For this reason, we adopt $E(B-V) = 0.78$ mag from the mean $B-V$ and $Q$ of Herbst and Feinstein. This provides a bolometric magnitude very close to those of the two O8.5 V stars Tr 16-115 and Tr 16-3, so we adopt the bolometric magnitude from these stars ($-6.8$ mag).

Figure 10 shows the $L_X/L_{bol}$ ratio for the stars in Table 6 as a function of spectral type. An approximate adjustment to the X-ray luminosities of HD 93162, Tr 16-244, and Tr 16-22 by a factor of 2.45 was made because of their larger reddening, which would correspond to an $E(B-V) = 0.90$ mag (estimated using PIMMS).

As is known from previous studies, for most stars in the O and early B spectral range the log of the $L_X/L_{bol}$ ratio remains constant at $-7$. There are three exceptions to this in Figure 10. The W-R star HD 93162 has been known since the X-ray discovery paper (Seward et al. 1979) to be unusually strong in X-rays, as compared with other W-R stars. This has been particularly surprising, as it has been thought to be a single star. Binaries with components this massive are often colliding-wind binaries and hence stronger X-ray sources than single stars. However, the recent W-R catalog by van der Hucht (2001) lists for the first time a possible binary indicator, "diluted emission lines." A companion bright enough to be detected photometrically would probably be luminous enough to have a wind that would enhance X-ray production.

Tr 16-22 (source 55) also has an unusually large X-ray luminosity in comparison with its bolometric luminosity [$\log(L_X/L_{bol}) \simeq -5.8$]. As noted above, it has a larger than average absorption, possibly because it is on the edge of the dust lane. However, the large X-ray luminosity suggests the source itself may have unusual characteristics beyond simple foreground reddening. The X-ray luminosity of the source [$L_X = (7.9 \pm 0.5) \times 10^{31}$ ergs s$^{-1}$ in Table 3, before the adjustment for high reddening], approximately a factor of 10 larger than that of other O8.5 V stars, makes it one of the brightest O stars observed.

The third source with a large $L_X/L_{bol}$ ratio is Tr 16-11, the B1.5 V star (source 141 in Table 1). Figure 10 shows that a B star would not even be detected unless it is unusually strong in X-rays. The luminosity [$L_X = (1.4 \pm 0.5) \times 10^{31}$ ergs s$^{-1}$] is within the range of the cool star distribution (Fig. 9), so a late companion is a possibility. MJ93 display its optical spectrum, which looks very like others of similar spectral type, except that perhaps the hydrogen lines are slightly broader.

The spread in the $L_X/L_{bol}$ ratio in Figure 9 is particularly large among the O3 stars. The two with the largest ratios are HD 93250 and Tr 16-244.

### 4.2. *Cool Stars*

The X-ray production in cool stars was similarly investigated using the X-ray luminosity (Table 4) and the optical luminosity from the data in Table 5. In this case, the typical extinction for the clusters [$E(B-V) = 0.52$ mag] was assumed for all the cool stars, as was the standard distance. Bolometric corrections were interpolated from Table 15.3.1 in Cox (2000, p. 338). The $V-I$ (Johnson) in that table was transformed to the Kron-Cousins system using the equations provided by Bessell (1979). The resulting plots of log $L_X$ and log ($L_X/L_{bol}$) as functions of $V-I$ are shown in Figures 11 and 12. For comparison, the colors of A0 V, F0 V, and K7 V stars (from Bessell 1979) are shown with the reddening of the clusters. Note that in this relatively short exposure we only detect a fraction of the stars in the cluster. For instance, presumably many M stars are not detected.

The most informative comparison is with comparable figures for the Orion Nebula cluster (ONC; *Chandra* results in Feigelson et al. 2002; *ROSAT* results in Gagné, Caillaut, & Stauffer 1995). Stars in the two regions are similar in age, although those in Tr 14 and Tr 16 are slightly younger (Meynet, Mermilliod, & Maeder 1993; Massey et al. 2001). Tr 14 and Tr 16 contain more massive stars than the ONC. Some X-ray sources among A stars are detected in both clusters. Feigelson et al. argue that because the $L_X$ distribution in late B and A stars is the same as for cooler stars, X-ray sources among late B and A stars can be explained by

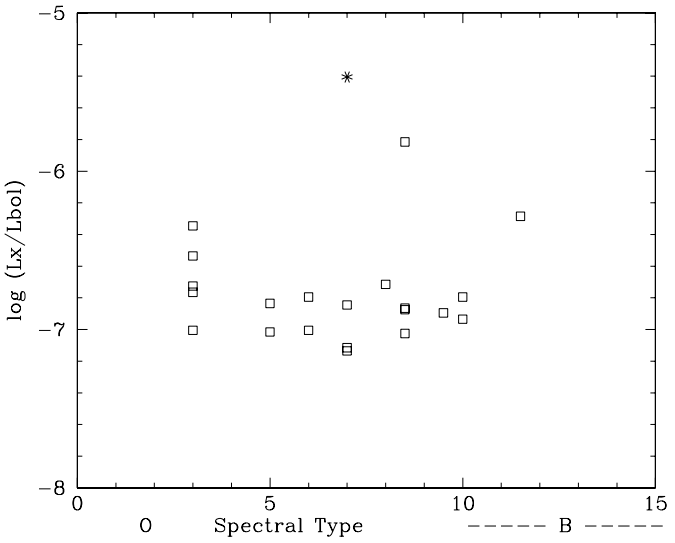



FIG. 10.—log ($L_X/L_{bol}$) as a function of spectral type for O and early B stars. O and B stars are marked by squares; the W-R star is marked by an asterisk, plotted at an arbitrary spectral type.

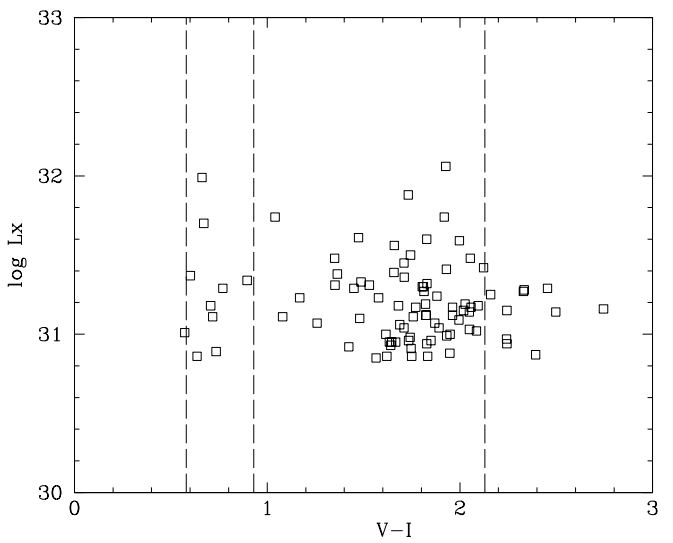



FIG. 11.—log $L_X$ as a function of $V-I$. Luminosity is in units of ergs s$^{-1}$. The vertical lines represent (*left to right*) the colors of A0 V, F0 V, and K7 V stars with the reddening of the clusters.

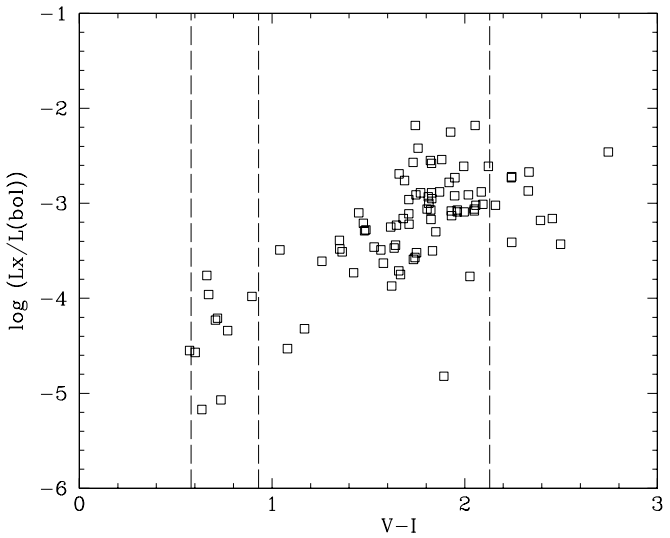



FIG. 12.—log ($L_X/L_{bol}$) as a function of $V-I$. Units of luminosity and definition of vertical lines as in Fig. 11.

less massive companions. Figure 11 shows the same result for Tr 14 and Tr 16.

## 5. DIFFUSE EMISSION

To illustrate diffuse emission in the field, a smoothed 0.3–7 keV image was created using the CIAO adaptive smoothing tool CSMOOTH. The result is shown in Figure 13, which indicates broad, diffuse emission from much of the nebula. We investigated the two circular regions 2′.5 in diameter marked in the figure: one centered 4′.0 south of $\eta$ Car and one centered 7′.5 south of HD 93129A/B. The figure shows seven unresolved sources in the first region, accounting for 30% of the emission after background subtraction. There are no unresolved sources in the second region.

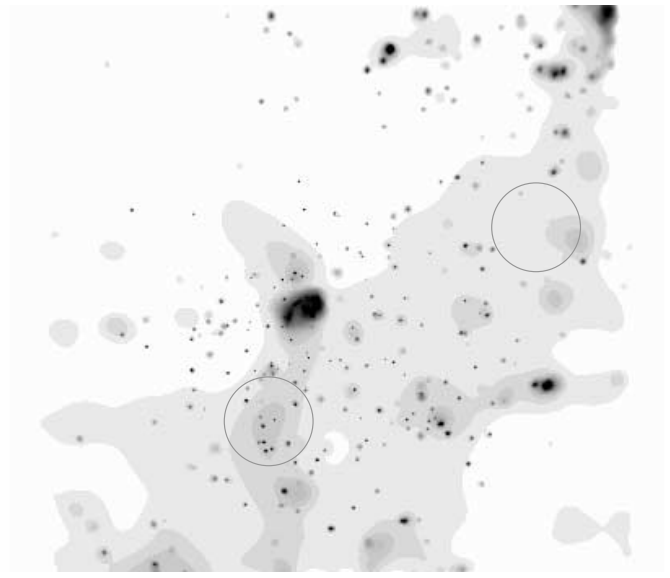


FIG. 13.—Smoothed image of the field to bring out the diffuse emission across the observation. The adaptive smoothing routine CSMOOTH was used. Circles indicate regions in which diffuse emission is discussed in the text.

After bright stars are subtracted, the residual above background in each region is ≈750 counts, or ≈150 counts arcmin$^{-2}$. This corresponds to a surface brightness of $\approx 2.5 \times 10^{-13}$ ergs cm$^{-2}$ s$^{-1}$ arcmin$^{-2}$ (unabsorbed). The luminosity of this region, if spherical, is $3 \times 10^{32}$ ergs s$^{-1}$ pc$^{-3}$

In the Orion Nebula (Garmire et al. 2000), one of the densest pre–main-sequence clusters known, the luminosity of X-ray–emitting stars in 1 pc$^3$ is $\sim 10^{32}$ ergs s$^{-1}$. Either the Carina region has a population of young stars denser than in most pre–main-sequence regions or much of this emission is truly diffuse. The X-ray spectra of these regions are thermal. If the regions have depth approximately equal to angular extent and the emission is due to diffuse, hot gas, over half the X-ray emission from the Carina Nebula originates in the diffuse component. A gas density of ∼0.5 particles cm$^{-3}$ is required. O star winds can easily supply the energy.

## 6. UPPER LIMITS TO UNDETECTED O AND B STARS

As is well known, B stars in general do not produce X-rays. Because of the extensive optical work that has been done on the stars in the two clusters, they provide a good place to explore the exact X-ray boundary. To do this, we have derived upper limits to the X-ray flux of the hot stars in Table 4 of MJ93 that are not detected in X-rays. Figure 14 shows the locations of these stars overlaid on the X-ray image. In Tr 16, in the center of the image, the circled locations appear to be free of sources. In Tr 14, in the upper right, the situation is more complex. Tr 14 is a crowded region, and sources in that region may have source confusion because of the large PSF off-axis.

We have adopted the criterion for source detection (§ 2) from Gehrels (1986). It is parameterized as a function of the number of background counts, which is a function of the off-axis distance. We have compared the measured counts at

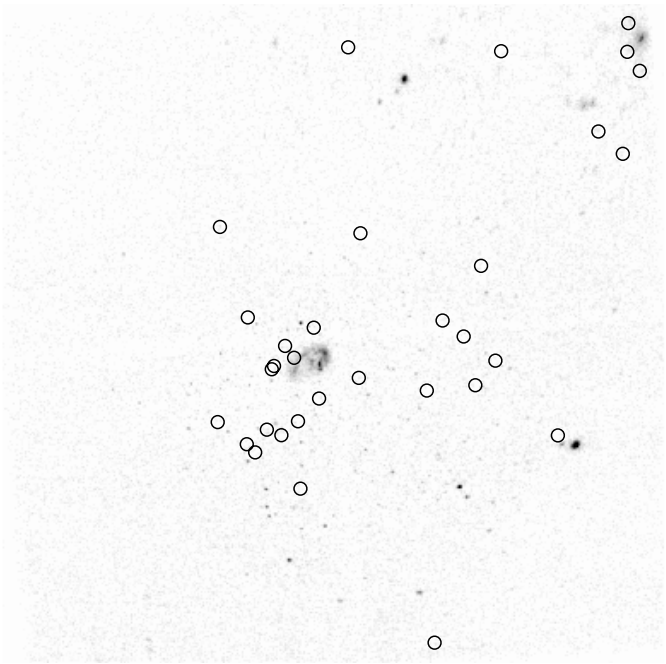


FIG. 14.—Hot stars *not* detected on the $\eta$ Car ACIS-I image. Circles are 30″ in diameter.

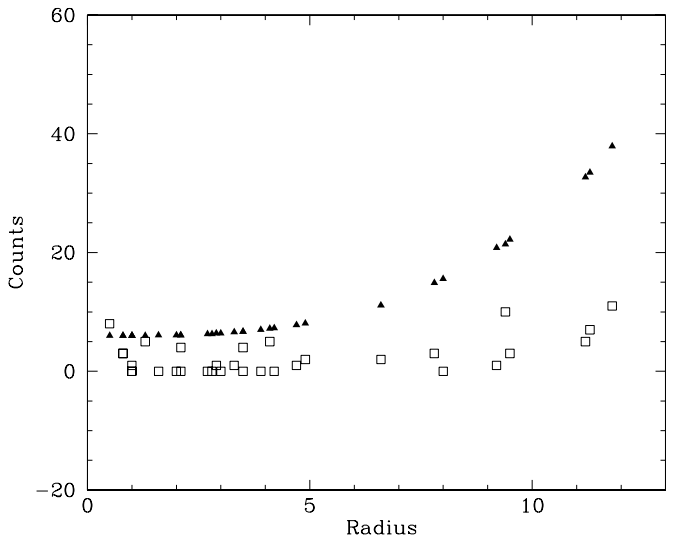



FIG. 15.—Counts at the positions of undetected hot stars. Squares show the counts within 2.″5 circles as a function of radial distance from the telescope axis (in arcminutes). Triangles show our detection criterion (see text) corresponding to each undetected source.

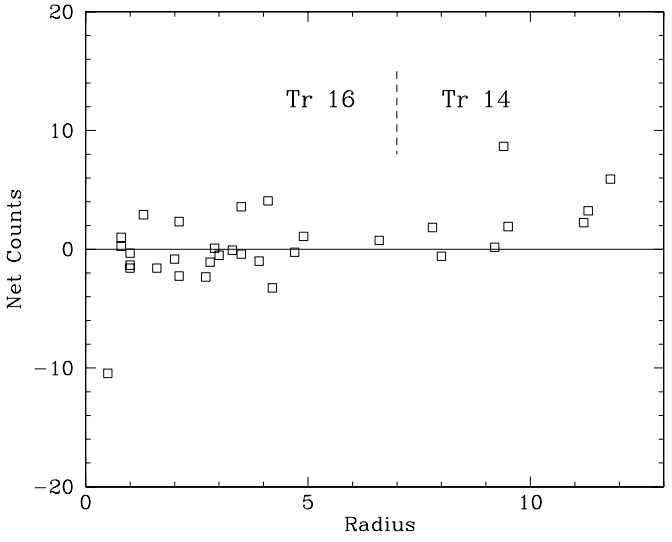



FIG. 16.—Net counts at the positions of undetected hot stars. Squares show the net counts within 2.″5 circles as a function of radial distance from the telescope axis (in arcminutes). (One point with very large net counts is omitted.) The approximate division between stars in Tr 16 (near the field center) and stars in Tr 14 is indicated.

the positions of the O and B stars in MJ93 (Table 4) that are not in Table 1 with the detection level predicted by the Gehrels criterion. Counts were measured in 2.″5 circles centered on these positions. For the center of the field, this is a generous allowance for the PSF (0.″68) plus an uncertainty in the pointing of 1″. Figure 15 shows that the measured counts are typically well below the detection criterion. (Note that the counts from which sources were selected for Tables 1–4 were based on WAVDETECT results; those in Fig. 13 are from extracted counts with no background subtraction.) The detection criterion used by Green et al. (1995) for a QSO survey is $C_{\rm src} \geq 4(C_{\rm bkg})^{1/2}$, where $C_{\rm src}$ and $C_{\rm bkg}$ are the counts in the source and background, respectively. For the very low background in the center of a 1 ks exposure, as seen in Figure 15, 1 background count corresponds to a detection limit of 4 source counts. As summarized in Figure 15, the Gehrels criterion provides a conservative upper limit for sources concealed in the measured counts.

Farther from the axis, the PSFs, and hence the included background counts, increase. For comparison with the detection criterion, counts for locations more than 7″ off-axis were measured in circles of 5″ and 10″ radius, as well as 2.″5 (not shown in Fig. 15). For radii less than 10′ off-axis, the PSF is less than 10″. Counts in the 10″ circles for several of the off-axis locations are above the detection criterion. As discussed below, there are probably actually sources at several of these locations. We note also that the Tr 14 region is a dense and complex one, and it is highly likely that additional sources are included as the measurement area is increased. Because of this complexity, further discussion of the upper limits far off-axis does not seem warranted.

With these explorations in mind, we adopt the Gehrels limit as the upper limit of counts at the location of early B stars.

The measured counts at the location of O and B stars from MJ93 Table 4 that are not detected sources are listed in Table 7. For each location, Table 7 provides the number (independent from the numbering in Tables 1–4), the position, the counts in the source and background areas, and the net counts, all with their errors. Counts are measured in a circle with a 5″ radius; background counts are measured in an annulus between radii of 5″ and 10″. Table 7 lists the radius from the aim point for each source and the spectral type (where available from MJ93). Spectral types are abbreviated to the temperature portion for plotting purposes. Upper limits to the luminosity (in units of ergs per second) are computed for the Gehrels criterion and the distance to the clusters.

Figure 16 shows the *net* counts at the location of hot stars. Counts were measured in a 2.″5 circle around the stellar positions. Background counts were measured an annulus between 5″ and 10″. The scatter around measures for Tr 16 near the center of the field is well balanced around zero, confirming that these are nondetections. For stars farther off-axis, the 2.″5 circle, of course, does not include the full PSF, and hence some source counts will be included in the region that defines the "background" counts. Even though the measures will be "overcorrected" for background, the Tr 14 stars have predominately positive source counts. This indicates that the central concentration in the PSF is such that a number of Tr 14 stars in fact are probably X-ray sources, even though they do not pass the detection criterion.

Figure 17 shows the upper limit luminosity from Table 6 for hot stars not detected in X-rays as a function of spectral type. The two O stars that were not detected have comparatively high upper limits because they are at the edge of the image. The counts corresponding to these upper limits are at or slightly above the lower envelope of the O star detections in Figure 5. Had they been at the image center, they might have been detected. On the other hand, the B stars from the center of the image have a typical count upper limit ($\log L_{\rm X} = 30.8$ ergs s$^{-1}$) that is below the counts of any detected hot star in Figure 8.

We can use Figure 4 to examine the dividing line between detected X-rays and the lack of X-rays. With the exceptions noted above, all O stars are detected. For the B0 spectral types, two stars are detected and one is not. Cooler B stars are not detected, with one exception. This points to a very

TABLE 7
NONDETECTIONS: OB STARS

| SOURCE | R.A. (J2000.0) | DECL. (J2000.0) | SOURCE AREA | | BACKGROUND AREA | | NET | | RADIUS (arcmin) | SPECTRAL TYPE | UPPER LIMIT OF $\log L_X$ |
|---|---|---|---|---|---|---|---|---|---|---|---|
| | | | Counts | Error | Counts | Error | Counts | Error | | | |
| 1..... | 10 43 59.96 | −59 32 26.3 | 30.0 | 5.5 | 61.0 | 7.8 | 9.6 | 6.1 | 11.8 | O6.5 | 31.613 |
| 2..... | 10 44 26.54 | −59 41 02.8 | 3.0 | 1.7 | 15.0 | 3.9 | −2.0 | 2.2 | 4.7 | B1.5 | 30.925 |
| 3..... | 10 44 38.73 | −59 48 14.3 | 6.0 | 2.4 | 14.0 | 3.7 | 1.3 | 2.7 | 7.8 | ... | 31.208 |
| 4..... | 10 44 56.27 | −59 33 04.0 | 2.0 | 1.4 | 7.0 | 2.6 | −0.3 | 1.7 | 8.0 | B0.5 | 31.228 |
| 5..... | 10 44 00.97 | −59 35 46.2 | 12.0 | 3.5 | 13.0 | 3.6 | 7.7 | 3.7 | 9.5 | O9 | 31.382 |
| 6..... | 10 45 08.99 | −59 40 40.7 | 6.0 | 2.4 | 24.0 | 4.9 | −2.0 | 2.9 | 0.8 | ... | 30.813 |
| 7..... | 10 44 40.38 | −59 41 49.0 | 2.0 | 1.4 | 6.0 | 2.4 | −0.0 | 1.6 | 3.0 | B1 | 30.843 |
| 8..... | 10 45 11.22 | −59 41 11.4 | 6.0 | 2.4 | 16.0 | 4.0 | 0.7 | 2.8 | 1.0 | B1 | 30.814 |
| 9..... | 10 44 32.94 | −59 40 26.1 | 4.0 | 2.0 | 12.0 | 3.5 | −0.0 | 2.3 | 3.9 | B1 | 30.880 |
| 10..... | 10 44 00.14 | −59 33 10.1 | 19.0 | 4.4 | 45.0 | 6.7 | 4.0 | 4.9 | 11.3 | ... | 31.560 |
| 11..... | 10 45 11.69 | −59 41 16.3 | 3.0 | 1.7 | 19.0 | 4.4 | −3.3 | 2.3 | 1.0 | ... | 30.814 |
| 12..... | 10 45 03.20 | −59 40 12.8 | 4.0 | 2.0 | 33.0 | 5.7 | −7.0 | 2.8 | 0.8 | B0.5 | 30.813 |
| 13..... | 10 44 30.56 | −59 41 40.6 | 3.0 | 1.7 | 39.0 | 6.2 | −10.0 | 2.7 | 4.2 | B1 | 30.896 |
| 14..... | 10 44 54.12 | −59 41 29.6 | 9.0 | 3.0 | 25.0 | 5.0 | 0.7 | 3.4 | 1.3 | B1 | 30.815 |
| 15..... | 10 45 02.16 | −59 42 01.3 | 6.0 | 2.4 | 16.0 | 4.0 | 0.7 | 2.8 | 1.0 | B1 | 30.814 |
| 16..... | 10 45 16.53 | −59 39 57.0 | 3.0 | 1.7 | 10.0 | 3.2 | −0.3 | 2.0 | 2.0 | ... | 30.821 |
| 17..... | 10 43 57.62 | −59 33 39.3 | 19.0 | 4.4 | 33.0 | 5.7 | 8.0 | 4.8 | 11.2 | B1 | 31.550 |
| 18..... | 10 44 05.86 | −59 35 12.2 | 14.0 | 3.7 | 16.0 | 4.0 | 8.7 | 4.0 | 9.4 | B1 | 31.365 |
| 19..... | 10 45 12.70 | −59 42 48.8 | 10.0 | 3.2 | 20.0 | 4.5 | 3.3 | 3.5 | 2.1 | B2 | 30.822 |
| 20..... | 10 44 25.52 | −59 33 09.9 | 4.0 | 2.0 | 10.0 | 3.2 | 0.7 | 2.3 | 9.2 | B1.5 | 31.353 |
| 21..... | 10 44 53.82 | −59 37 48.5 | 4.0 | 2.0 | 5.0 | 2.2 | 2.3 | 2.1 | 3.5 | B2 | 30.859 |
| 22..... | 10 45 05.93 | −59 44 19.0 | 5.0 | 2.2 | 13.0 | 3.6 | 0.7 | 2.5 | 3.3 | B2 | 30.852 |
| 23..... | 10 45 07.17 | −59 40 58.7 | 50.0 | 7.1 | 221.0 | 14.9 | −23.8 | 8.6 | 0.5 | ... | 30.813 |
| 24..... | 10 44 29.47 | −59 38 38.0 | 3.0 | 1.7 | 11.0 | 3.3 | −0.7 | 2.1 | 4.9 | B1 | 30.943 |
| 25..... | 10 44 37.22 | −59 40 01.6 | 8.0 | 2.8 | 5.0 | 2.2 | 6.3 | 2.9 | 3.5 | B0.5 | 30.860 |
| 26..... | 10 44 13.85 | −59 42 57.1 | 3.0 | 1.7 | 15.0 | 3.9 | −2.0 | 2.2 | 6.6 | B0 | 31.080 |
| 27..... | 10 45 22.14 | −59 37 38.8 | 10.0 | 3.2 | 11.0 | 3.3 | 6.3 | 3.4 | 4.1 | B2 | 30.891 |
| 28..... | 10 45 15.05 | −59 43 23.4 | 4.0 | 2.0 | 13.0 | 3.6 | −0.3 | 2.3 | 2.8 | ... | 30.835 |
| 29..... | 10 45 09.78 | −59 42 57.2 | 2.0 | 1.4 | 27.0 | 5.2 | −7.0 | 2.2 | 2.1 | B1 | 30.822 |
| 30..... | 10 45 16.76 | −59 43 11.0 | 2.0 | 1.4 | 28.0 | 5.3 | −7.3 | 2.3 | 2.7 | ... | 30.834 |
| 31..... | 10 45 22.62 | −59 42 37.0 | 5.0 | 2.2 | 11.0 | 3.3 | 1.3 | 2.5 | 2.9 | ... | 30.838 |
| 32..... | 10 45 06.39 | −59 42 35.9 | 1.0 | 1.0 | 19.0 | 4.4 | −5.3 | 1.8 | 1.6 | ... | 30.817 |

NOTE.—Units of right ascension are hours, minutes, and seconds, and units of declination are degrees, arcminutes, and arcseconds.

clean divide in spectral type at B0. It also provides us with a list of 14 stars in Tr 16 for which we can constrain the properties of a cool companion star. This upper limit only overlaps with the weakest sources in the distribution of X-ray luminosities (Fig. 9). While we would not yet have detected a companion comparable to the faintest X-ray sources among late-type cluster members, we can say that the B stars do not have X-ray–bright companions.

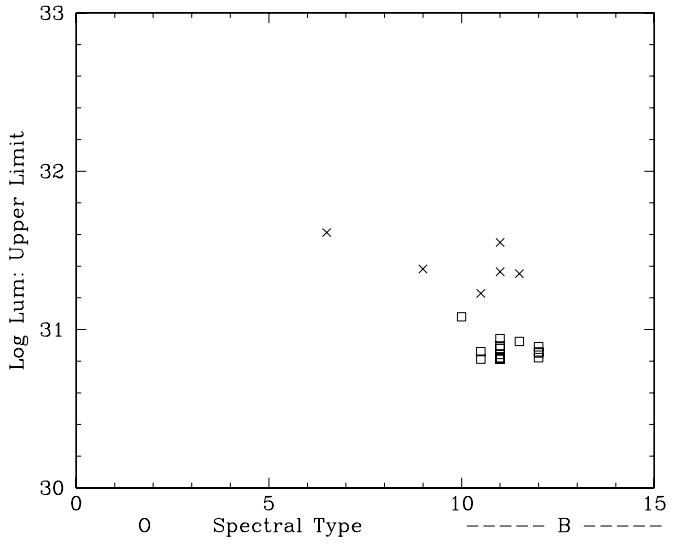



FIG. 17.—Upper limit to $\log L_X$ in units of ergs cm$^{-1}$ for undetected hot stars as a function of spectral type. Crosses mark stars more than 7′ from the aim point (Tr 14); squares mark stars closer than 7′ (Tr 16).

## 7. HARDNESS RATIOS

The hardness ratios of X-ray sources provide the simplest description of their spectra. In this section, we explore the hardness ratios (Tables 3 and 4) as defined in § 2 for both hot stars and other X-ray sources. We limit the sources examined to the brightest, so the errors in the ratios are small enough that they do not obscure any trends or comparisons. We have examined the distribution of errors in the hardness ratios as a function of luminosity. For the OB stars (Table 3), if we use only sources with $\log L_X \geq 32.2$ ergs s$^{-1}$, the uncertainty in the soft hardness ratio, $HR_{MS}$, is less than or equal to 0.1 (with one exception); for the hard hardness ratio, $HR_{HM}$, the error is less than or equal to 0.15. The other stars (Table 4, referred to as cool stars below) are somewhat weaker in X-rays than the hot stars, so we use sources with $\log L_X \geq 32.0$ ergs s$^{-1}$. This results in uncertainties less than 0.2 in both colors (after two sources with large errors were removed from the sample). Our sample is thus limited to only the brightest sources.

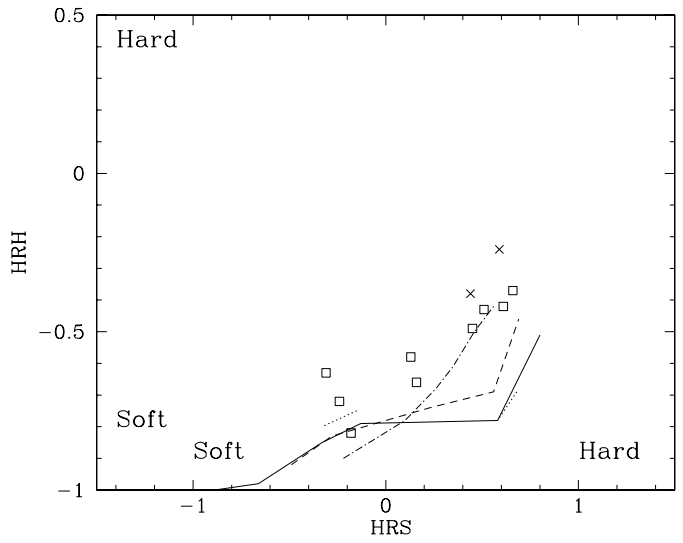



FIG. 18.—Hardness ratio "color-color" diagram. HRH is the hardness ratio from the hard and medium energy bands ($HR_{HM}$), HRS that from the medium and soft bands ($HR_{MS}$). See text for discussion. Squares mark OB stars and crosses other sources, presumably pre–main-sequence stars. The solid line shows hardness ratios created using PIMMS for Raymond-Smith plasma for a variety of temperatures for solar abundance; the dashed line is for 0.2 solar abundance. The dot-dashed line is from thermal bremsstrahlung, also for a range of temperatures. The dotted lines shows the effect of varying the extinction (Raymond-Smith, solar abundance) from $N_H = 3 \times 10^{21}$ to $5 \times 10^{21}$ cm$^{-2}$, corresponding approximately to the range of $E(B-V)$ in the field from 0.5 (standard) to 0.9 mag (exceptional). The dotted line near HRS −0.2 has been raised by 0.05 in HRH, so that it is not completely hidden by the thermal locus.

Figure 18 shows the resulting hardness ratio plot. The hardness ratio created from the soft and medium bands (0.5–0.9 and 0.9–1.5 keV) can be either positive or negative, i.e., either band can have more counts, whereas the hardness ratio from the medium and hard band (1.5–2.04 keV) is always negative, i.e., the hard band always has fewer counts. The hot stars fall in a diagonal sequence, with a scatter consistent with the uncertainties in the colors. There are only two cool stars with well-determined hardness ratios, which are both very hard in Figure 18.

We have explored this locus further by creating hardness ratios in the same bands using PIMMS (version 3.2). The basic model (solid line in Fig. 18) is a Raymond-Smith model with solar abundance and a temperature range from $\log T = 6.0$ to 7.2. A neutral column density $N_H = 3 \times 10^{21}$ cm $^{-2}$ was used corresponding to the typical extinction for the field $E(B-V) = 0.52$ mag. For two temperatures, $N_H$ was increased to $5 \times 10^{21}$ cm $^{-2}$, corresponding to $E(B-V) = 0.9$ mag, an extreme value found for a few stars in the field. The result of this difference in extinction is shown in Figure 18. For comparison, we have computed hardness ratios for 0.2 solar abundance (dashed line in Fig. 18). We have also computed models for thermal bremsstrahlung ($kT$ from 0.2 to 1.0 keV). Figure 18 shows that a range of $HR_{MS}$ (the soft ratios) can be obtained with any of the models. However, the observed ratios for both hot and cool stars lie systematically at larger (harder) values of $HR_{HM}$ than the computed values for either Raymond-Smith plasma or bremsstrahlung. Although the bremsstrahlung ratios for the hottest temperature match the ratios for the hot stars, for cooler temperatures they are a poorer match than the Raymond-Smith models. Based on these models, the $HR_{MS}$ values for the hot stars indicate a range of temperatures from approximately $3 \times 10^6$ to more than $10^7$.

How are these X-ray hardness ratios related to the optical (photospheric) properties of the stars? In Figure 18, the three hot stars with negative $HR_{MS}$ are HDE 303308 [$E(B-V) = 0.46$ mag; O3 V], HD 93205 [$E(B-V) = 0.40$ mag; O3 V], and CPD $-59^\circ 2600$ [$E(B-V) = 0.51$ mag; O6 V]. In other words, all three have reddening typical of the field. The stars with $HR_{MS}$ near 0.1 are HD 93250 [$E(B-V) = 0.49$ mag; O3 V] and HD 93160 [$E(B-V) = 0.31$ mag; O6 III]. Interpreting the hardness ratios in terms of photospheric temperature arrives at the contradiction that the X-ray temperatures are hotter than the O3 V stars in the first group, although the photospheric temperatures are similar or cooler. The four hot stars with distinctly harder $HR_{MS}$ are Tr 16-22 [O8.5 V, $E(B-V) = 0.78$ mag], Tr 16-244 [O3 I, $E(B-V) = 0.94$ mag], HD 93129A/B [O3 I, $E(B-V) = 0.55$ mag], and HD 93162 [=WR 25; WN7+abs, $E(B-V) = 0.66$ mag]. None of these are normal main-sequence objects. Both HD 93129A/B and Tr 16-22 are among the hottest stars known (O3) and also very luminous. The fact that HD 93129A/B apparently has the normal reddening for Tr 14 suggests that the very hard $HR_{HM}$ does not result from circumstellar material. This is in contrast to Tr 16-244, which has the same temperature and luminosity but is more heavily reddened than the average cluster member. Both HD 93162 and Tr 16-22 stand out in Figure 10 because they have a particularly large $L_X/L_{bol}$. We already know that HD 93162 is unusual, since not only has it evolved to be a very early stage in the W-R sequence, but it is also unusually X-ray–luminous for a W-R star. Tr 16-22, on the other hand, is cooler and fainter than stars evolving off the main sequence in the clusters. Its unusually hard and bright X-ray luminosity must be linked with some unusual property, such as a massive binary companion.

The two cool stars with well-determined hardness ratios are both among the hardest stars in the field. Interestingly, one is located within the range of the cool pre–main-sequence stars in Figure 7, but one is one of the X-ray–bright A stars.

Figure 19 confirms that the $HR_{MS}$ (the soft hardness ratio) is not correlated with photospheric temperature indicated by spectral type. The O3 stars, in particular, cover a very large range in $HR_{MS}$.

How do we interpret the hardness ratios of the X-ray sources in Tr 14 and Tr 16? There seem to be two important considerations. First, we are looking at a biased sample. Because we have restricted the sample to sources with reasonably well-determined ratios, we are only looking at the most luminous sources. Second, both the hot and cool stars have more counts in the hard band than predicted from the simple PIMMS calculations. A plausible interpretation for this is that we have used a one-temperature model in the calculations, but the sources may actually have a second, harder component. This is frequently seen in spectral fits of stellar sources. We note that the discussion of the individual sources above rules out single-parameter explanations of the hardness based on photospheric temperatures or circumstellar reddening. In summary, unusually X-ray–bright sources are surprisingly hard.

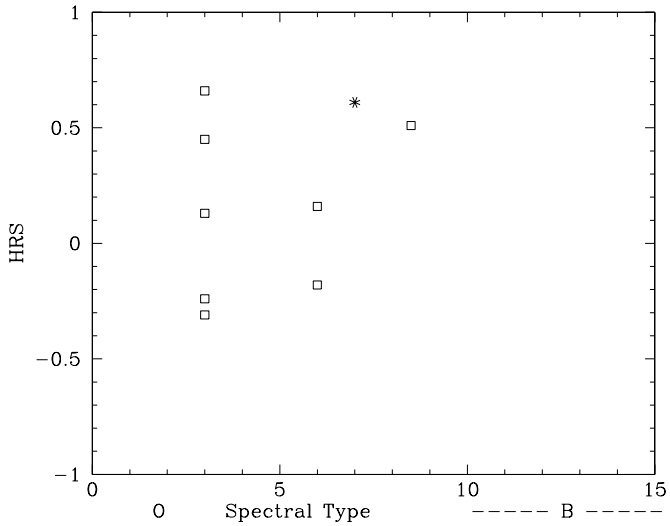



FIG. 19.—Soft hardness ratio $HR_{MS}$ as a function of spectral type for the hot stars. Squares mark O stars; the W-R star has been arbitrarily plotted as an asterisk at O7. Soft colors are at the bottom.

## 8. DISCUSSION

### 8.1. *Binaries*

We have assembled the X-ray properties of sources in Tr 14 and Tr 16, including several sources that are unusually strong or hard in X-rays. We have already discussed properties such as reddening, spectral type, and luminosity in relation to the X-ray properties. One further property (at least) may be important in X-ray production, namely, whether the star is single, a member of a close binary system, or a member of a wide binary system.

In O stars, a binary companion with sufficient mass to drive a wind of its own may enhance X-ray production via a "colliding wind." A good deal of work has been done to establish whether the stars in the Carina clusters are single or multiple. The most definitive study, with the highest resolution spectra, is that of Penny et al. (1993). They concluded that none of the six bright members of Tr 14 are short-period spectroscopic binaries. This is in contrast to an earlier study at lower resolution by Levato et al. (1991a). However, the Penny work and a later study by García et al. (1998) demonstrate that Tr 14 is surprisingly deficient in short-period binaries among the hottest stars. Penny et al. suggest that the cluster has remained compact because the lack of binaries lowers the cluster heating via binary-binary interactions, although the results come from, of course, only the brightest stars.

Velocity studies of 26 stars in Tr 16 were carried out by Levato et al. (1991b), using the same equipment used for the Tr 14 study, with relatively low resolution (43 Å $mm^{-1}$). They found velocity variation in at least 50% of the stars studied. The work by this team in Tr 14 was superseded by higher resolution work, and the radial velocity variations they found in Tr 16 need to be confirmed. It would be quite surprising to have dramatically different binary fractions in the two clusters. Three of the X-ray sources in the ACIS field have recently been observed by the X-Mega campaign to obtain optical spectroscopy of the hot stars that are X-ray sources. Albacete Colombo et al. (2001) have observed CPD $-59°2635$. They found that it is a double-lined spectroscopic binary and determined an orbit. Both components are massive, and Albacete Colombo et al. determine spectral types of O8 V and O9.5 V. HD 93205 has been observed by Morrell et al. (2001), who report that it is another double-lined spectroscopic binary with O3 V and O8 V components. CPD $-59°2636$ is a triple system, with O7 V, O8 V, and O9 V components (Albacete Colombo et al. 2002). Components A and B are a binary with a period of 3.6 days. Component C is itself a binary with a period of 5.0 days. CPD $-59°2603$ (=Tr 16-104) has been observed by Rauw et al. 2001. They find it to be a triple system with O7 V, O9 V, and B0.2 IV components. The close binary (O7 V and O9 V stars) has a period of 2.2 days and short eclipses.

Recently E. Nelan et al. (2002, private communication) have resolved HD 93129A with the *Hubble Space Telescope* FGS (fine guidance system). This may affect the X-ray properties, although the two components are much more widely separated than the binaries in Table 8, so it is not clear that it does.

We have collected radial velocity information about the single/binary nature of the X-ray sources in the field in Table 8. It shows the hot stars within the *Chandra* field, the source of velocity information, the binary status, and the orbital period where available. Mason et al. (1998) provide a convenient summary of velocity work on a number of these stars and also speckle interferometry to sample wider binaries. In Table 8, we have marked the velocity variations from Levato et al. (1991b) with colons to indicate that they need confirmation.

Identifying multiple systems in hot stars with broad lines is not easy. In addition to the radial velocity studies, as

TABLE 8
BINARIES: VELOCITIES

| Star | Binary Status | $P_{orb}$ (days) | Reference |
|---|---|---|---|
| HD 93129A | N | ... | 1 |
| HD 93129B | N | ... | 1 |
| HD 93250 | N | ... | 2 |
| HD 93205 | Y | 6.1 | 2, 3 |
| HD 93160 | Y | ... | 2 |
| HD 93162 | ... | ... | |
| HDE 303308 | Y: | ... | 2 |
| HD 93204 | N | ... | 2 |
| CPD $-59°2600$ | N | ... | 2 |
| CPD $-59°2603$ | Y | 2.2 | 2 |
| HDE 303311 | N | ... | 2 |
| CPD $-59°2635$ | Y | 2.3 | 4 |
| CPD $-59°2641$ | Y: | 4.0 | 2 |
| CPD $-59°2636$ | Y | 3.6, 5.0 | 5 |
| CPD $-59°2628$ | Y: | 5.8 | 2 |
| HD 93343 | Y: | ... | 2 |
| Tr 16-9 | N | ... | 2 |
| Tr 16-10 | Y: | ... | 2 |
| Tr 16-23 | N | ... | 2 |
| Tr 16-115 | N | ... | 2 |
| Tr 16-3 | N | ... | 2 |
| Tr 16-244 | ... | ... | |
| Tr 16-22 | ... | ... | |
| Tr 16-11 | ... | ... | |

REFERENCES.—(1) Penny et al. 1993; (2) Levato et al. 1991b; (3) Morrell et al. 2001; (4) Albacete Colombo et al. 2001; (5) Albacete Colombo et al. 2002.

discussed above, van der Hucht (2001) has suggested that the W-R star HD 93162 may be a binary, on the basis of diluted emission lines. Penny (1996) has suggested that HD 93250 might be a binary, on the basis of variable line widths. This is in accord with the suggestion of a companion (Walborn, Nichols-Bohlin, & Panek 1985) based on unsaturated C IV line cores. Confirmation of the single/multiple status of HD 93250 is a very important question in the interpretation of the X-ray flux of this extremely luminous object.

Table 8 can be used to compare what is known about the single/binary nature of X-ray sources that are unusually strong, using, for instance, log ($L_X/L_{bol}$) in Table 6. For the W-R star HD 93162, $L_X$ is particularly strong, but evidence for a binary system is only indirect. Among the O3 stars, HD 93250 is a strong, and also hard, X-ray source and again has only indirect evidence of a possible binary companion. HD 93129A/B is a strong, and also hard, X-ray source, although its $L_X/L_{bol}$ is not remarkable. There is no evidence for a close binary companion. Tr 16-22 is a remarkably strong X-ray source, but it does not have radial velocity studies. On the other hand, HD 93205, which is a double-lined spectroscopic binary (Morrell et al. 2001) with an orbital period of 6.1 days and spectral types of O3 V and O8 V, is not a particularly strong X-ray source. CPD $-59^\circ 2635$ is also a double-lined spectroscopic binary (Albacete Colombo et al. 2001), with a period of 2.3 days and spectral types O8 V and O9.5 V, and again is not a particularly strong X-ray source. CPD $-59^\circ 2636$ is a similar case of a multiple system with two short-period binaries (Albacete Colombo et al. 2002) but an unremarkable X-ray flux. In summary, the two with particularly hard spectra (HD 93129A/B and HD 93250) may well not be binaries. On the other hand three sources in short-period binaries made up of O star components (HD 93205, CPD $-59^\circ 2635$, and CPD $-59^\circ 2636$) are not particularly remarkable X-ray sources.

The emerging picture is that while close binaries with two hot stars may produce a strong X-ray flux (the colliding-wind model), this does not seem to be the whole explanation for surprisingly strong X-ray sources. Clearly, there is the standard problem that there is almost never enough information to prove that a star is single. However, it is short-period binaries with massive companions that should be colliding-wind systems, and they are the easiest to find. With the incomplete velocity evidence that is available, strong sources and binary orbits are nearly anticorrelated. We suspect this demonstrates that our knowledge of binary systems is incomplete.

HD 93162 (=WR 25) and HD 93250 are surprisingly strong in X-rays, but with only indirect suggestions of a binary companion. Should it turn out that the X-ray strength does come from a companion, this would provide an important way to get more complete statistics on the binary fraction in massive stars, since such strong X-ray sources are not overlooked.

Chlebowski & Garmany (1991) provide comparisons of X-ray flux and stellar parameters, such as wind velocity and luminosity, for an extensive list of O stars. They find that in general binaries do not produce larger mass loss than single stars. On the other hand, close binaries seem to produce more X-ray flux than either contact binaries or wider binaries. One way to reconcile these trends with the apparent lack of correlation between binary status in Table 8 and excess X-ray flux is that we are sampling regimes where different effects become dominant. This is particularly likely for the group of extreme stars found in the Carina Nebula: the most massive and the most luminous. For instance, for the most massive stars, extreme mass-loss rates may dominate over binary/single trends and produce an unusually large X-ray flux. For stars less massive than O3 stars, the effect of a close binary with a massive companion may become evident in the X-ray flux.

### 8.2. *HD 93250*

As summarized above, there is no *velocity* evidence that HD 93250 is a short-period binary system, although there are suspicions that it might have a companion from line width variations and line depths. However, the recent re-examination by Walborn et al. (2002) stresses line depth in the context of luminosity, not companions. This paper stresses that complications in the interpretation of these extreme stars because of binary companions must be understood using Milky Way examples. Even though there are many examples in the Magellanic Clouds, observations are typically contaminated by a surrounding cluster. If HD 93250 is single (and there is no clear evidence at present against this), it is a pivotal object in understanding the X-ray production and evolution of very massive stars. It is an extremely strong (and also hard) X-ray source in comparison with other O3 stars. Among the Tr 14 and Tr 16 stars it has a $V$ magnitude second only to that of HD 93129A/B (MJ93). The hardness ratio $HR_{MS}$, however, lies between those of the softer O3 stars and the harder but unusual and more luminous HD 93129A/B and Tr 16-244. If X-ray flux of HD 93250 is not affected by a companion, it provides a benchmark of an extremely luminous main-sequence dwarf with a very high $L_X/L_{bol}$ produced by the outer atmosphere processes of the star itself. Since it will presumably accelerate its mass loss as it evolves off the main sequence, it provides an important example of high X-ray production of a star before its mass loss becomes extreme.

### 8.3. *B Stars*

There is another regime in which X-ray observations provide an important handle on the binary fraction in massive stars. The upper limits to X-rays from B stars (Fig. 17) apply also to the X-ray flux from a cool companion. For instance, the upper limit to the luminosity ($\log L_X = 30.8$ ergs s$^{-1}$) would pick up many of the cool star X-ray sources in the ONC (Feigelson et al. 2002). In other words, a deeper image could rule out most cool companions. Quantifying what fraction of companions would be detected at a given sensitivity level, however, is not easy. We can estimate from Figure 10 of Feigelson et al. that less than a quarter of the Orion cool stars would be detected with the sensitivity limit of our $\eta$ Car image (including a small approximate correction to account for absorption in Orion). However, Figure 12 of Feigelson et al. implies that companions of A and late B stars have a higher luminosity than the average cool star. That is, for a given sensitivity limit, a larger fraction of companions would be detected than estimated from the luminosity distribution of late-type stars. Accurately identifying binary companions much less massive than the primary is very difficult to do, particularly for massive B stars with only a few broad lines to measure velocities from. X-ray studies provide detection of this otherwise elusive population of companions.

### 8.4. *Colliding-Wind Binaries*

The emerging picture of colliding-wind binaries is that they include systems with widely separated components, as well as systems with close components. WR 140, with an orbital period of 8 yr, is an example. Our summary of velocity information about binaries in Table 8 and the discussion in § 8.1 indicate that the relation between binary status and strong X-rays is not simple. The recent *XMM-Newton* spectrum of the W-R star WR 110 (Skinner et al. 2002) suggests yet another complication in interpretation. They find a cool, soft component to the spectrum, as expected from a wind-shock model, and in addition they find a hard X-ray component. They examine a number of possibilities for producing this component and conclude that it can be produced by a wind and a close but as yet undetected companion. However, if the companion is not found, they suggest the possibility that the hard component is produced by the W-R star itself.

## 9. SUMMARY

The *Chandra* image of $\eta$ Car and the clusters Tr 14 and Tr 16 has provided a number of new results.

1. Although the hottest stars have been known to be X-ray sources since the *Einstein Observatory* observations, this is the first time the population of X-ray sources associated with cooler stars has been discussed.

2. Two new, anomalously strong X-ray sources have been found among the hot star population. Tr 16-244, a heavily reddened O3 I star, and Tr 16-22, a heavily reddened O8.5 V star, have surprisingly large X-ray fluxes. They are both close to the dust lanes that cross the sides of the cluster and may be responsible for the above-average reddening.

3. Several stars have an unusually large $L_X/L_{bol}$. HD 93162, a W-R star, has long been known to have an even higher $L_X/L_{bol}$ than other W-R stars. There is some indication that it may be a binary, which could account for this. Tr 16-22 also stands out in $L_X/L_{bol}$, perhaps indicating a colliding-wind binary, although there are no radial velocity studies to provide further information. The third star with a large $L_X/L_{bol}$ is Tr 16-11, the B1.5 star. The X-ray flux may be produced by a second, cool star.

4. We confirm that the OB stars are on average more luminous than the other X-ray sources that are pre–main-sequence stars, as has been found in other regions.

5. The X-ray sources (cool stars) define a locus in the color-magnitude diagram that lies above stars that are presumably field stars in the Carina arm.

6. We have put upper limits on the OB stars in the field that we do not detect. For comparison, in this short exposure, if companions to the B stars had an X-ray luminosity distribution like that of the late-type stars in the ONC, we would detect only a fraction of the companions.

7. We discuss the hardness ratios of the brightest sources in bands 0.5–0.9, 0.9–1.5, and 1.5–2.04 keV, although the sample is limited to only the brightest sources. Hardness ratios are not correlated in a simple way with photospheric temperature (spectral type). Both hot and cool stars lie parallel to a locus derived for an isothermal plasma; however, there is an offset, indicating extra counts in the highest energy band. This could be due to a second component at a higher temperature, at least for these very luminous sources.

8. We summarize the information available about the binary orbital velocity motion of the O star X-ray sources.

It is a pleasure to thank everyone who worked on the *Chandra* project for making these data possible. We thank Nuria Huelamo (MPE) for obtaining optical images of the field. Useful comments were provided by D. Gies. We thank an anonymous referee for comments that improved the presentation of the results. Financial assistance was provided from the *Chandra* X-ray Center NASA contract NAS 8-39073.

## REFERENCES

Albacete Colombo, J. F., Morrell, N. I., Niemela, V. S., & Corcoran, M. F. 2001, MNRAS, 326, 78
Albacete Colombo, J. F., Morrell, N. I., Rauw, G., Corcoran, M. F., Niemela, V. S., & Sana, H. 2002, MNRAS, 336, 1099
Baraffe, I., Chabrier, G., Allard, F., & Hauschildt, P. H. 1998, A&A, 337, 403
Bessell, M. S. 1979, PASP, 91, 589
Chlebowski, T. 1989, ApJ, 342, 1091
Chlebowski, T., & Garmany, C. D. 1991, ApJ, 368, 241
Corcoran, M. F., Swank, J., Rawley, G., Petre, R., Schmitt, J., & Day, C. 1995, Rev. Mexicana Astron. Astrofis. Ser. Conf., 2, 97
Cox, A. N., ed. 2000, Allen's Astrophysical Quantities (4th ed.; New York: Springer)
Crowther, P. A., Hillier, D. J., & Smith, L. J. 1995a, A&A, 293, 403
Crowther, P. A., Smith, L. J., Hillier, D. J., & Schmutz, W. 1995b, A&A, 293, 427
Cudworth, K. M., Martin, S. C., & DeGioia-Eastwood, K. 1993, AJ, 105, 1822
Davidson, K., & Humphreys, R. M. 1997, ARA&A, 35, 1
Feigelson, E. D., Broos, P., Gaffney, J. A., III, Garmire, G., Hillenbrand, L. A., Pravdo, S. H., Townsley, L., & Tsuboi, Y. 2002, ApJ, 574, 258
Feinstein, A. 1969, MNRAS, 143, 273
Gagné, M., Caillault, J.-P., & Stauffer, J. R. 1995, ApJ, 445, 280
García, B., Malaroda, S., Levato, H., Morrell, N., & Grosso, M. 1998, PASP, 110, 53
Garmire, G., Feigelson, E. D., Broos, P., Hillenbrand, L. A., Pravdo, S. H., Townsley, L., & Tsuboi, Y. 2000, AJ, 120, 1426
Gehrels, N. 1986, ApJ, 303, 336
Green, P. J., et al. 1995, ApJ, 450, 51
Harnden, F. R., Jr., et al. 1979, ApJ, 234, L51
Herbst, W. 1976, ApJ, 208, 923
Levato, H., Malaroda, S., García, B., Morrell, N., & Solivella, G. 1991a, Ap&SS, 183, 147
Levato, H., Malaroda, S., Morrell, N., García, B., & Hernández, C. 1991b, ApJS, 75, 869
Mason, B. D., Gies, D. R., Hartkopf, W. I., Bagnuolo, W. G., Jr., ten Brummelaar, T., & McAlister, H. A. 1998, AJ, 115, 821
Massey, P., DeGioia-Eastwood, K., & Waterhouse, E. 2001, AJ, 121, 1050
Massey, P., & Johnson, J. 1993, AJ, 105, 980 (MJ93)
Massey, P., Waterhouse, E., & DeGioia-Eastwood, K. 2000, AJ, 119, 2214
Meynet, G., Mermilliod, J.-C., & Maeder, A. 1993, A&AS, 98, 477
Morrell, N. I., et al. 2001, MNRAS, 326, 85
Penny, L. R. 1996, ApJ, 463, 737
Penny, L. R., Gies, D. R., Hartkopf, W. I., Mason, B. D., & Turner, N. H. 1993, PASP, 105, 588
Rauw, G., Sana, H., Antokhin, I. I., Morrell, N. I., Niemela, V. S., Albacete Colombo, J. F., Gosset, E., & Vreux, J.-M. 2001, MNRAS, 326, 1149
Seward, F. D., Butt, Y. M., Karovska, M., Prestwich, A., Schlegel, E. M., & Corcoran, M. 2001, ApJ, 553, 832
Seward, F. D., & Chlebowski, T. 1982, ApJ, 256, 530
Seward, F. D., Forman, W. R., Giacconi, R., Griffiths, R. E., Harnden, F. R., Jr., Jones, C., & Pye, J. P. 1979, ApJ, 234, L55
Skinner, S. L., Zhekov, S. A., Güdel, M., & Schmutz, W. 2002, ApJ, 572, 477
Tapia, M., Roth, M., Marraco, H., & Ruiz, M. T. 1988, MNRAS, 232, 661
Turner, D. G., & Moffat, A. F. J. 1980, MNRAS, 192, 283
van der Hucht, K. A. 2001, NewA Rev., 45, 135
Walborn, N. R. 1971, ApJ, 167, L31

Walborn, N. R. 1995, Rev. Mexicana Astron. Astrofis. Ser. Conf., 2, 51
Walborn, N. R., Nichols-Bohlin, J., & Panek, R. J. 1985, *International Ultraviolet Explorer* Atlas of O-Type Spectra from 1200 to 1900 Å (NASA RP-1155; Washington: NASA)
Walborn, N. R., et al. 2002, AJ, 123, 2754
Weisskopf, M. C., Brinkman, B., Canizares, C., Garmire, G., Murray, S., & Van Speybroeck, L. P. 2002, PASP, 114, 1
Willis, A. J., & Crowther, P. A. 1996, in Wolf-Rayet Stars in the Framework of Stellar Evolution, ed. J.-M. Vreux, A. Detal, D. Fraipont-Caro, E. Gosset, & G. Rauw (Liège: Univ. de Liège), 109